

4

AFGL-TR-89-0045  
ENVIRONMENTAL RESEARCH PAPERS, NO. 337

PROTEL: Design, Fabrication, Calibration, Testing, and Satellite  
Integration of a Proton Telescope

AD-A214 564

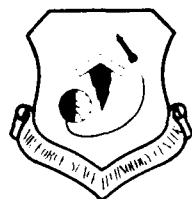
KRISTINA A. LYNCH, Capt, USAF  
EDWARD A. BOUGHAN  
DAVID K. FISCHI  
DAVID A. HARDY  
KEVIN B. RIEHL, Capt, USAF



16 February 1989



Approved for public release; distribution unlimited.



DTIC  
ELECTE  
NOV 27 1989  
S B D



SPACE PHYSICS DIVISION

PROJECT 7601


**AIR FORCE GEOPHYSICS LABORATORY**

HANSCOM AFB, MA 01731

89 11 21 136

"This technical report has been reviewed and is approved for publication."

FOR THE COMMANDER

  
(Signature)

EDWARD G. MULLEN, Chief  
Space Particles Environment Branch

  
(Signature)

RITA C. SAGALYN, Director  
Space Physics Division

This report has been reviewed by the ESD Public Affairs Office (PA) and is releasable to the National Technical Information Service (NTIS).

Qualified requestors may obtain additional copies from the Defense Technical Information Center. All others should apply to the National Technical Information Service.

If your address has changed, or if you wish to be removed from the mailing list, or if the addressee is no longer employed by your organization, please notify AFGL/DAAC, Hanscom AFB, MA 01731. This will assist us in mailing a current mailing list.

Do not return copies of this report unless contractual obligations or notices on a specific document requires that it be returned.

UNCLASSIFIED

SECURITY CLASSIFICATION OF THIS PAGE

## REPORT DOCUMENTATION PAGE

Form Approved  
OMB No. 0704-0188

1a. REPORT SECURITY CLASSIFICATION Unclassified			1b. RESTRICTIVE MARKINGS N/A	
2a. SECURITY CLASSIFICATION AUTHORITY			3. DISTRIBUTION / AVAILABILITY OF REPORT Approved for public release; distribution unlimited.	
2b. DECLASSIFICATION / DOWNGRADING SCHEDULE				
4. PERFORMING ORGANIZATION REPORT NUMBER(S) • AFGL-TR-89-0045 ERP, No. 337			5. MONITORING ORGANIZATION REPORT NUMBER(S)	
6a. NAME OF PERFORMING ORGANIZATION Air Force Geophysics Laboratory		6b. OFFICE SYMBOL (If applicable) PHP	7a. NAME OF MONITORING ORGANIZATION	
6c. ADDRESS (City, State, and ZIP Code) Hanscom AFB Massachusetts 01731-5000			7b. ADDRESS (City, State, and ZIP Code)	
8a. NAME OF FUNDING / SPONSORING ORGANIZATION		8b. OFFICE SYMBOL (If applicable)	9. PROCUREMENT INSTRUMENT IDENTIFICATION NUMBER	
8c. ADDRESS (City, State, and ZIP Code)			10. SOURCE OF FUNDING NUMBERS	
			PROGRAM ELEMENT NO. 62101F	PROJECT NO. 7601
			TASK NO. 22	WORK UNIT ACCESSION NO. 02
11. TITLE (Include Security Classification) PROTEL: Design, Fabrication, Calibration, Testing, and Satellite Integration of a Proton Telescope				
12. PERSONAL AUTHOR(S) Lynch, K.A., Capt, USAF; Boughan, E.A.*; Fischl, D.K.**; Hardy, D.A., Riehl, K.B., Capt, USAF				
13a. TYPE OF REPORT Scientific Interim		13b. TIME COVERED FROM _____ TO _____	14. DATE OF REPORT (Year, Month, Day) 1989 February 16	15. PAGE COUNT 86
16. SUPPLEMENTARY NOTATION *MIT, Center for Space Research; ** MIT/Lincoln Laboratory				
17. COSATI CODES			18. SUBJECT TERMS (Continue on reverse if necessary and identify by block number)	
FIELD	GROUP	SUB-GROUP	CRRES; radiation belts; proton environment; particle detectors (solid state)	
19. ABSTRACT (Continue on reverse if necessary and identify by block number) A high energy proton telescope, PROTEL, was designed, fabricated, calibrated, tested, and integrated as part of the SPACERAD experiment for the joint Air Force/NASA Combined Release and Radiation Effects Satellite (CRRES) payload. As designed, PROTEL measures the differential energy spectrum of protons in 24 channels logarithmically spaced from 1 to 100 MeV, and the approximate flux of heavy ions. It consists of a Data Processing Unit (DPU), and two sensor head assemblies (High and Low Energy Head). The active elements of the sensor heads are stacked arrays of silicon-lithium drifted and surface barrier solid state detectors. This report describes the basic design, the command system, and the telemetry format of PROTEL, as well as the test and calibration results for the detector head assemblies and electronic logic system obtained with several accelerators. Also described are results of computer modeling of the response of the instrument, particularly the estimation of pulse pileup and efficiency.				
20. DISTRIBUTION/AVAILABILITY OF ABSTRACT <input checked="" type="checkbox"/> UNCLASSIFIED/UNLIMITED <input type="checkbox"/> SAME AS RPT. <input type="checkbox"/> DTIC USERS			21. ABSTRACT SECURITY CLASSIFICATION Unclassified	
22a. NAME OF RESPONSIBLE INDIVIDUAL Dr. David A. Hardy			22b. TELEPHONE (Include Area Code) (617) 377-3211	22c. OFFICE SYMBOL AFGL/PHP

## Preface

Grateful acknowledgement is made of assistance from Robert Redus, Marilyn Oberhardt, and Timothy Schumaker, who worked long hours at various instrument calibrations; and from Nick Vickers and David Kelleher, who spent their summers reducing calibration and test data.

Accession For		
NTIS GRA&I	<input checked="" type="checkbox"/>	
DTIC TAB	<input type="checkbox"/>	
Unannounced	<input type="checkbox"/>	
Justification		
By		
Distribution/		
Availability Codes		
Dist	Avail and/or	Special
A-1		

## Contents

1. INTRODUCTION	1
1.1 Overall Description	1
1.2 Previous Instrumentation	2
2. INSTRUMENT DESCRIPTION	3
2.1 Overall Purpose	3
2.2 Mechanical Design	6
2.3 Logic System and Data Format	16
2.4 Electronics, Commands, and Telemetry	26
2.4.1 Electronics Design	26
2.4.2 Commands and Telemetry	28
2.5 Operation	34
3. CALIBRATION AND TESTING	38
3.1 Brief Overview of Calibration Procedures	38
3.2 Individual Detector Testing and Calibration	38
3.2.1 Low Energy Head Detectors	38
3.2.2 High Energy Head Detectors	41
3.3 Environmental Testing	43
3.4 Accelerator Beam Calibrations - Procedures and Setup	47
3.5 Satellite Integration	59
3.6 Refurbishment and Recalibration	59
3.7 Calibration Results	60
4. COMPUTER SIMULATIONS	71
4.1 Introduction	71
4.2 Pulse Pileup Simulation	71
4.3 Response Function Simulations	71
REFERENCES	77

## Illustrations

1. High Energy Sensor Head	7
2. Low Energy Sensor Head	8
3. Detector Guard Rings	
a. HD1	13
b. HD2-5	14
4. High Energy Head Detector Stack	15
5. PROTEL Mounted on Spacecraft	17
6. Deposited vs. Incident Energy Curves	
a. Graph of Energy Deposited in a Silicon Slab vs. Incident Proton Energy	19
b. Graph of Energy Deposited in Each of the Detectors in the High Energy Stack vs. Incident Particle Energy	20
c. Same as 5b, but for the Low Energy Head	21
d. Same as 5b, but for the Low Energy Head Heavy Ions	22
7. Science Data Display	24
8. Housekeeping Data Display	25
9. Block Diagram of DPU Electronics	27
10. Spacecraft Telemetry Stream - One Minor Frame	32
11. Science Data Word Construction	35
12. Science Data Word Telemetry Locations	36
13. Preliminary Detector Test Setup	39
14. Alpha Source Test Setup	42

## Illustrations

15. Thermal Vacuum Test Setup	45
16. Thermal Vacuum Test Cycles	46
17. Thermal Test Cycles	48
18. Accelerator Calibration Setup	58
19. HEH Efficiency Curves	65
20. LEH Efficiency Curves	67
21. STRAGGL Routine Response for HEH	73
22. STRAGGL Routine Response for LEH	74

## Tables

1. Channel Boundaries and Coincidence Logic	
a. High Energy Sensor Head	4
b. Low Energy Sensor Head	5
c. Heavy Ion Channels - Low Energy Head	5
2. Detector Characteristics	
a. High Energy Head	10
b. Low Energy Head	11
3. General Information	18
4. Command Matrix Cells and Mnemonics	29
5. Analog Signals and Mnemonics	33
6. Calibration Sequence	37
7. Leakage Currents	40
8. Alpha Source Characteristics	40
9. Shock and Vibration Test Specifications	44
10. Pittsburgh Van de Graaf Accelerator Runs	49
11. Princeton Accelerator Runs	55
12. Harvard Cyclotron Runs	56
13. Empirical Channel Boundaries - HEH	
a. Pittsburgh Data	61
b. Princeton Data	62
c. Harvard Data	62



## Tables

14.	Empirical Channel Boundaries - LEH	63
15.	Empirical Channel Boundaries - Ions	64
16.	Deposition Ratios	
a.	HEH Deposition Ratios	68
b.	LEH Deposition Ratios	69
17.	Average Channel Efficiencies	70

# **PROTEL: Design, Fabrication, Calibration, Testing and Satellite Integration of a Proton Telescope**

## **1. INTRODUCTION**

### **1.1 Overall Description**

Microelectronic components in satellite instrumentation can be adversely affected by the near Earth radiation environment either from accumulated dose or from single event upsets. The effect of the space radiation environment on microelectronic components is one of the primary limiting factors on the capabilities of present and planned space systems. In order to better study the interaction of the space radiation environment with such systems, the SPACERAD experiment was designed and built for flight on the joint Air Force/NASA Combined Release and Radiation Effects Satellite (CRRES).

SPACERAD is an experiment in which the operation of state-of-the-art electronic components will be monitored as they are exposed to the Earth's radiation belt environment. That environment will be monitored by an array of 18 on-board instruments. Data from these instruments will be used to determine the relationship between the behavior of the devices under test and the history of the

---

(Received for publication 13 February 1989)

radiation environment to which the components were exposed. In addition, the environmental monitors will create a large data base for use in the development of both static and dynamic radiation belt models.

PROTEL is one of these environmental monitors. It was designed to measure the differential energy spectrum of 1 to 100 MeV protons in 24 logarithmically spaced channels. PROTEL consists of a Data Processing Unit (DPU) and two sensor heads. The High Energy Sensor Head (HEH) measures 6 - 100 MeV protons in 16 approximately contiguous channels, and the Low Energy Sensor Head (LEH) measures 1 - 9 MeV protons in 8 channels. The entire 24 point spectrum is returned once per second. In addition, the Low Energy Head returns some data on the flux of heavy ions.

PROTEL has been extensively calibrated, using both alpha particle sources and proton and ion beam accelerators. The measured energy depositions and response efficiencies have been tabulated and compared to the results of a computer simulation.

This report consists of: 1) a description of PROTEL, including its design, data format, and operation; 2) the calibration and testing procedure and results; and 3) a description of the computer simulations for energy deposition, response efficiency, and pulse pileup, with a comparison of the calibration data to the simulation results.

## 1.2 Previous Instrumentation

In recent years, only a few instruments have measured protons in the 1-100 MeV range, and even fewer have made these measurements through the center of the radiation belts. As a result, present radiation belt models<sup>1</sup> are based mostly on data from instruments flown in the 1960s. Protons in the energy range from 5.6 to 46 MeV were measured by the University of Kiel S-30 instrument on the polar orbiting German DIAL satellite.<sup>2</sup> This instrument used a collimated telescope and a pair of solid state detectors with a large geometric factor. Data were obtained from March to May of 1970. The Lockheed High Energy Proton Spectrometer (HEPS) consisted of a silicon detector stack, a 20 degree half angle collimator, and a scintillator guard. The instrument, measuring protons from 1.2 to 100 MeV, was flown on the polar orbiting STP 71-2 satellite.<sup>3</sup> AFGL provided instruments for the OV5-6, S3-2, and S3-3 satellites in the period from 1969 to 1976. These devices consisted of a collimated telescope with two solid state detectors to measure protons from 5 to 100 MeV. The instruments had significant

- 
1. Vette, J.L., Teague, M.J., Sawyer, D.M., and Chan, K.W. (1979) Modeling of the Earth's radiation belts, *Solar Terrestrial Predictions Proceedings* (Vol. 2), R.F. Donnelly, Ed., U.S. Dept. of Commerce, Washington, D.C.
  2. Fischer, H.M., Auschrat, V.W., and Wibberenz, G. (1977) Angular distribution and energy spectra of protons of energy  $5 < E < 50$  MeV at the lower edge of the radiation belt in equatorial latitudes, *J. Geophys. Res.* **82**:537.
  3. Reagan, J.B., Bakke, J.C., Kilner, J.R., Mathews, J.D., and Imhoff, W.L. (1972) A high-resolution multiple-particle spectrometer for the measurements of solar particle events, *IEEE Trans. Nucl. Sci.* **NS-19**:554.

background problems.<sup>4,5,6</sup> The Los Alamos Charged Particle Analyzer, (CPA), flown on the 1976-059A satellite, consisted of two sensor heads measuring protons at geosynchronous altitude in the energy range from 145 keV to 150 MeV. Each sensor head had a collimator, a sweeping magnet, solid state detectors, and shielding.<sup>7,8</sup>

With PROTEL's design, we have endeavored to incorporate the strengths of previous instruments, while avoiding past problems, such as background noise, with heavy shielding and many coincidence requirements. With 24 channels and careful, extensive calibration, the instrument will provide a high resolution proton spectrum for the CRRES orbit.

The PROTEL sensor elements are solid state silicon detectors, both surface barrier and silicon-lithium drifted. For more information about these detectors, see Brown<sup>9</sup>, Knoll<sup>10</sup>, and EG&G Ortec's guide to their surface barrier detectors.<sup>11</sup>

## 2. INSTRUMENT DESCRIPTION

### 2.1 Overall Purpose

PROTEL was designed to return well calibrated, high resolution proton flux data over incident energies from 1 to 100 MeV. The data are obtained with two sensor head units, one covering the energy range from 1 to 9 MeV and the other from 6 to 100 MeV. The spectrum is measured in 24 discrete channels, spaced at approximately equal logarithmic intervals in incident energy, with the full spectrum returned once each second. The width of each channel is approximately 20% of the channel's central energy for the high energy assembly, and 33% for the low energy assembly. In addition, the instrument returns some data on the flux of heavy ions by counting, in five channels, the number of particles depositing from 6 MeV to 60 MeV in the Low Energy Head detector 1. Tables 1a - 1c show the nominal channel boundaries and coincidence logic schemes for both assemblies.

- 
4. Morel, P.R., Hanser, F.A., and Sellers, B. (1974) *A Satellite Telescope for Protons and Alphas*, Panametrics, Inc., Waltham, Mass., Final Report for AFCRL-TR-74-0531, AD A003727.
  5. Parsignault, D.R., Holeman, E., and Filz, R.C. (1981a) Solar cycle induced modulation of the 55 MeV proton fluxes at low altitudes, *J. Geophys. Res.* **86**:11493.
  6. Parsignault, D.R., Holeman, E., and Filz, R.C. (1981b) Long term intensity decrease in the 8- to 25- MeV proton fluxes at low L values, *J. Geophys. Res.* **86**:11447.
  7. Belian, R.D., Baker, D.N., Higbie, P.R., and Hones, E.W., Jr. (1978) High-resolution energetic particle measurements at 6.6  $R_E$ . 2. High-energy proton drift echoes, *J. Geophys. Res.* **83**:4857.
  8. Baker, D.N., Belian, R.D., Higbie, P.R., and Hones, E.W., Jr. (1979) High-energy magnetospheric protons and their dependence on geomagnetic and interplanetary conditions, *J. Geophys. Res.* **84**:7138.
  9. Brown, W.L., Higgenbotham, W.A., Miller, G.L., and Chase, R.L. (1969) *Semiconductor Nuclear Particle Detectors and Circuits*, National Academy of Sciences, Publication 1594, Washington, D.C.
  10. Knoll, G. (1979) *Radiation Detection and Measurement*, John Wiley and Sons, New York, N.Y.
  11. EG&G Ortec, *Silicon Charged Particle Radiation Detectors Instruction Manual*, EG&G Ortec, Oak Ridge, Tennessee.

Table 1a. Channel Boundaries and Coincidence Logic  
High Energy Sensor Head

<p>Ei is the proton incident energy (MeV); the columns under D# list the amount of energy (keV) deposited in detector HD# by a particle with incident energy Ei. #&gt;&gt; is the channel number between the incident energy channel borders. The deposited energies shown are those in the active detector thickness only; thus they will not add up to the given incident energy Ei because of losses in shielding, absorbers, and dead layers. In region (L) the particles either are stopped in previous detectors or do not deposit enough energy to trigger the later detectors. In region (N), D2 and D3 are not considered by the logic. Note that these tables list the desired discriminator settings; the actual empirical settings are listed in Tables 14-16.</p>					
Ei	D1	D2	D3	D4	D5
6.00	2.376				
1>> 7.50	4.776				
2>> 9.48	7.50	0.994		(L)	
3>> 10.14	4.818	3.074			
4>> 11.53	3.768	5.875			
5>> 14.92	2.712	11.00	1.024		
6>> 15.75		7.346	4.228		
7>> 18.08		5.465	9.058		
8>> 24.715		3.589	18.90	0.998	
9>> 27.22			11.891	9.587	
10> 34.915			7.746	23.00	1.029
11> 37.82				14.322	12.298
12> 48.145		(N)		9.031	30.75
13> 53.54				7.837	17.632
14> 62.08				6.643	13.032
15> 73.12				5.447	10.221
16> 100.00	0.478			4.252	7.283

Table 1b Channel Boundaries and Coincidence Logic  
Low Energy Sensor Head

Same as Table 1a, but for the Low Energy Sensor Head.				
E1	D1	D2	D3	D4
1.000	.477			
1>>				
1.960	1.470	.490	(L)	
2>>				
2.232	.945	1.006		
3>>				
2.750	.741	1.580	.496	
4>>				
3.108	.653	.951	1.282	
5>>				
3.940	-	.671	2.417	.486
6>>				
4.683	-		1.340	2.176
7>>				
7.210	-	(N)	.765	5.668
8>>				
9.000	-		.610	3.154

Table 1c. Channel Boundaries and Coincidence Logic  
Heavy Ion Channels - Low Energy Head

The heavy ion measurement system uses only one detector, but measures several types of particles. Table 1c has only one column for deposited energy, and it is the deposited not the incident, energies which define the channel boundaries. The other columns list incident energies for various species of particle corresponding to each deposited energy.				
Channel	Edep	EI-C	EI-O	EI-Fe
	6.0	19.0	26.0	62.0
5>>				
	15.0	27.0	36.0	85.0
6>>				
	29.0	-	46.0	105.0
7>>				
	36.0	-	50.0	110.0
8>>				
	44.0	-	-	125.0
9>>				
	60.0	-	-	140.0

The active elements of the sensor heads are stacks of silicon transmission detectors. A proton entering through the collimator of one of the sensor heads will pass through the stack of detectors until it has lost all its energy. The amount of energy deposited in each detector is analyzed by the logic system. The event is listed in the science data display format as a raw count, and if the logic determines it to be valid, as a count in an energy channel as well. In addition, the housekeeping monitors keep track of the status of the instrument at all times.

The raw data are formatted for telemetry downlink by the data processing unit (DPU). After spacecraft downlink, they are formatted into two displays. The science data display lists the raw count rates, the count rates partly converted to events, and the actual processed counts per channel per second. Raw counts are monitored in addition to the true channel count events because the relationship between the two is a measure of the efficiency of the instrument. The second display format of data, the housekeeping display, monitors the status of the instrument itself, tracking the voltages and temperatures and the status of the command system. Both displays are discussed in more detail in Section 2.3.

The telemetry returns a complete set of science data every second, and a fully updated housekeeping display every sixteen seconds. The high resolution proton spectra shown in the science data display will be a major element of the CRRES data base.

## 2.2 Mechanical Design

The basic design of the two sensor heads is the same. Each has a front collimator, a sweeping magnet to reject high energy electrons, an entrance and an exit aperture, a detector stack, and various background shielding schemes. Figures 1 and 2 show the two assemblies.

The collimator, which is made of aluminum, is designed to eliminate most of the proton and electron flux coming from outside the desired angular acceptance cone. The angular acceptance cone of the collimator is matched to that defined by the diameters of the detectors in the stack. The half angle opening of the collimator is  $16.90^\circ$  ( $9.67^\circ$ ) for the high (low) energy head. The thinnest portion of the collimators has a range, for orthogonally impinging protons, of 42 (37) MeV. For protons hitting the collimator outside the acceptance cone, but in a direction that would impinge upon the detector stack, this range is of the order of several hundred MeV. The inside surface of the collimator is cut in a sawtooth pattern to reduce the forward scattering of particles into the entrance aperture.

The sweeping magnet, located between the entrance and exit apertures, is designed to remove any electron flux which would otherwise produce background in the proton data. The maximum field strength for the high (low) sensor head magnet is approximately 5 kgauss, which will sweep out electrons of up to 8 MeV (4 MeV) in energy.

The entrance and exit apertures of the high (low) energy sensor head are constructed such that the acceptance angle as determined by the detector diameters is  $16.70^\circ$  ( $9.53^\circ$ ). The area of each aperture is  $1.76 \text{ cm}^2$  ( $0.552 \text{ cm}^2$ ). Given the separation between the entrance and exit apertures, the geometric factor of the sensor head is  $.12 \text{ cm}^2\text{-ster}$  ( $.0121 \text{ cm}^2\text{-ster}$ ), using the formula

$$G = .5 \pi^2 \{ (2R^2 + d^2) - (4R^2 d^2 + d^4)^{1/2} \}$$

# PROTEL - HIGH ENERGY RANGE (6 - 100 MeV)

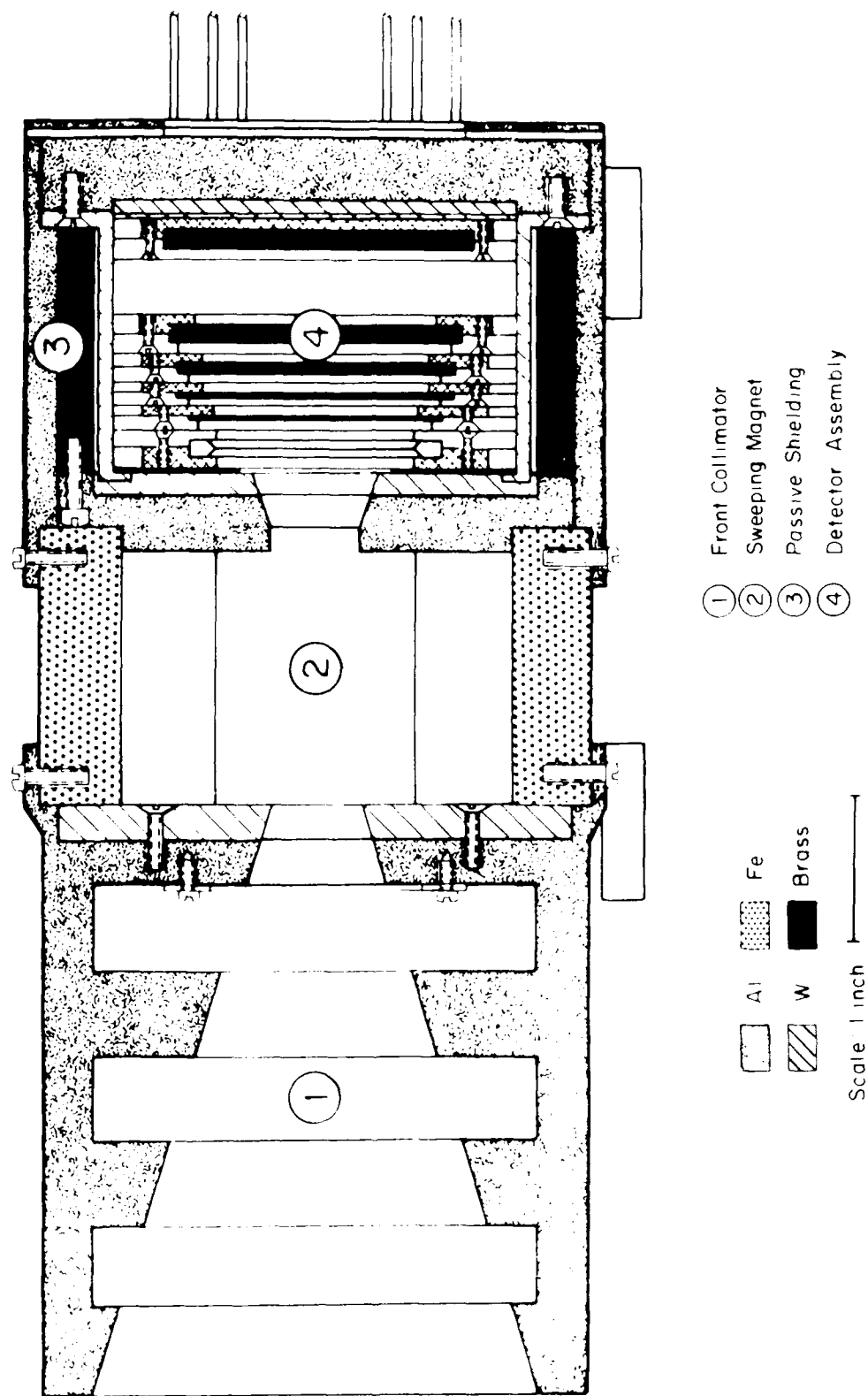


Figure 1. High Energy Sensor Head



# PROTEL - LOW ENERGY RANGE (1-9 MeV)

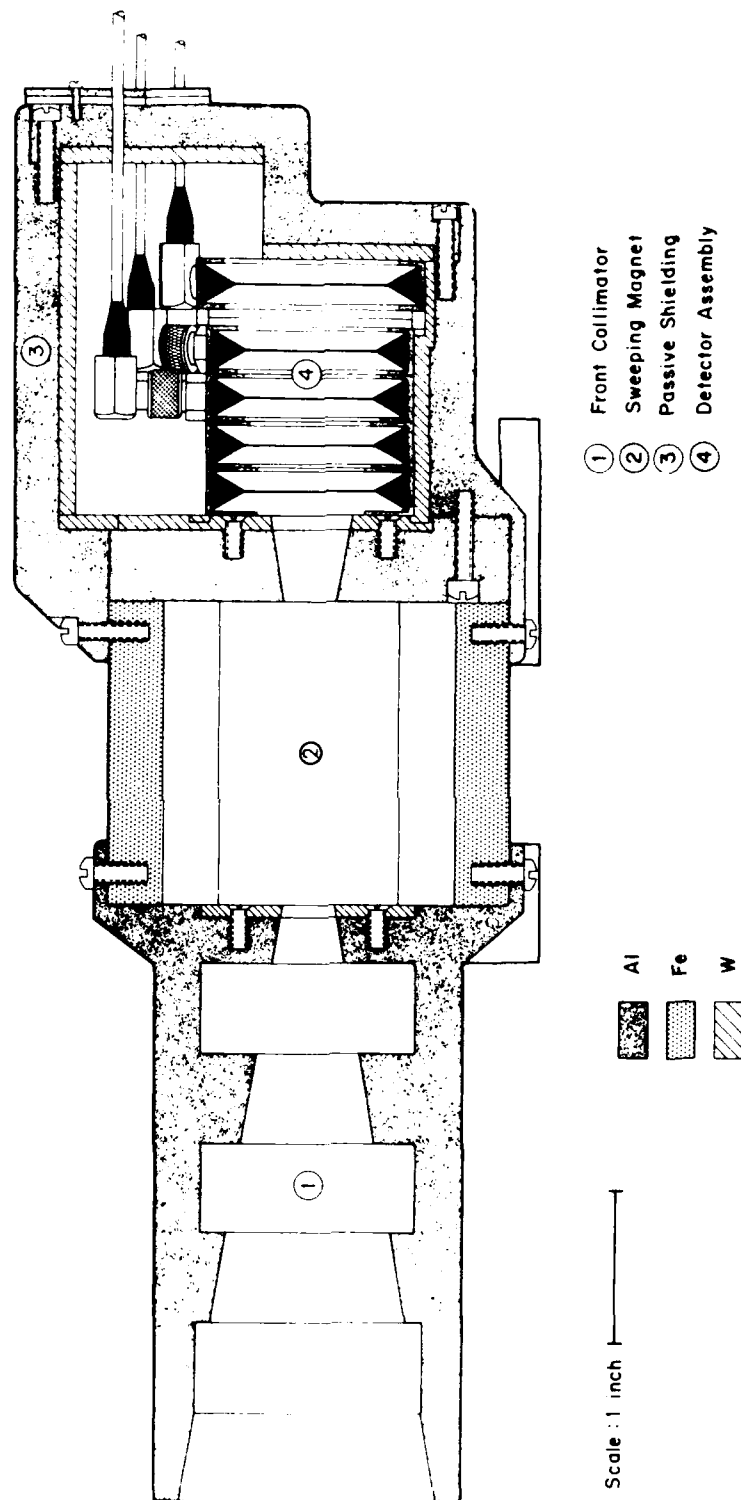


Figure 2. Low Energy Sensor Head

where  $R$  is the radius of the apertures and  $d$  is the distance between them.<sup>12</sup>

The entrance aperture is cut through 0.744 (0.747) cm of aluminum and 0.681 (0.254) cm of tungsten alloy. The exit aperture is cut through 0.318 (1.17) cm of aluminum and 0.681 (0.254) cm of tungsten alloy.

Behind the apertures are the solid state detectors. Two types of detectors are used, silicon-lithium drifted (SILi) detectors manufactured by Lawrence Berkeley Laboratories, and surface barrier detectors manufactured by EG&G Ortec in Tennessee. A summary of the detector characteristics is given in Tables 2a and 2b. Two types of detectors are needed because of the wide range of energies being measured. Thin surface barrier detectors are required for the finer absolute resolution measurements of the Low Energy Head. Larger, thicker silicon-lithium drifted detectors are needed for the higher energy depositions of the High Energy Head measurements. Both types of detectors employ a slab of silicon wafer which is coated on one side with aluminum and on the other side with gold.

The surface barrier detectors are made by etching the silicon surface and evaporating a thin gold layer onto it. The process results in a slight oxidation of the silicon surface, which is an important factor in the operation of the detector. Because surface barrier transmission detectors have a very thin dead layer when fully depleted as these are, the maximum possible measurement is made of the loss of energy of a particle passing through the detector.<sup>13</sup> For more information on these detectors, see EG&G Ortec's guide to their surface barrier detectors.<sup>11</sup>

Surface barrier detectors have a maximum thickness limitation because of breakdown caused by the high reverse bias voltages needed for large depletion thicknesses. When longer stopping ranges are necessary, silicon-lithium drifted detectors are used. These detectors are made by diffusing lithium gas through one side of a silicon wafer. The wafer is then coated with evaporated gold on one side and aluminum on the other. Because of the lithium on one side, there is a significant dead layer in these detectors, which will increase with the age of the detector. Measurements must account for the fact that deposition is measured only in the active part of the thickness of the detector. However, these detectors are used because they can be made much thicker than surface barrier detectors.<sup>14</sup> For more information about these detectors see Brown<sup>8</sup> and Knoll.<sup>10</sup>

The high energy sensor head uses six detectors, designated HD1 through HD6 (for High energy head Detector #). The first is a surface barrier detector with a guard ring anti-coincidence shield. The others are all SILis, with guard rings (except for the last, which has no ring). The first five detectors are used to determine the incident proton energy. The sixth is separated from the others by a brass absorber and is used in anti-coincidence with the others to define the upper threshold energy of 100 MeV, and to veto particles entering from behind the stack.

The low energy sensor head uses five surface barrier detectors, designated LD1 through LD5. The first four are used to determine the incident proton energy. The fifth is separated from the others by

- 
12. Sullivan, J.D. (1971) Geometrical factors and directional response of single and multi-element particle telescopes, *Nuclear Instruments and Methods* **95**:5.
  13. Knoll, G. (1979) *Radiation Detection and Measurement*, John Wiley and Sons, New York, N.Y., p. 386.
  14. Knoll, G. (1979) *Radiation Detection and Measurement*, John Wiley and Sons, New York, N.Y., p. 415.

Table 2a. Detector Characteristics  
High Energy Head

All of the Low Energy Head detectors and HD1 are Ortec surface barrier detectors. The other High Energy Head detectors are Lawrence Berkeley Laboratory Silicon Lithium drifted detectors. NOTE: These specifications are for the detectors used during calibration and testing.						
	HD1	HD2	HD3	HD4	HD5	HD6
Serial Number	AB045900350S (EG&G)	5821 (LBL)	5833 (LBL)	5843 (LBL)	5852 (LBL)	5863 (LBL)
Thickness ( $\mu\text{m}$ )	390	788	2088	2083	5004	2986
Bias Voltage	100V	200V	300V	400V	600V	400V
Active Area Diam. (mm)	27.45	29.4	32.2	35.6	41.3	48.2
Guard Ring Inner Diam. (mm)	30.45	30.4	33.2	36.6	42.3	-
Guard Ring Outer Diam. (mm)	36.45	37.0	40.0	42.0	47.9	-
Mounting Case Diam. (mm)	46.48	46.18	49.17	51.16	57.15	57.15
Lithium Dead Layer ( $\mu\text{m}$ ) (when new)	-	13.3	11.5	13.3	8.4	12.2

Table 2b. Detector Characteristics  
Low Energy Head

All of the Low Energy Head detectors and HD1 are Ortec surface barrier detectors. The other High Energy Head detectors are Lawrence Berkeley Laboratory Silicon Lithium drifted detectors. NOTE: These specifications are for the detectors used during calibration and testing.					
	LD1	LD2	LD3	LD4	LD5
EG&G Serial Number	25-457E	25-458G	25-459I	25-460D	25-461D
Thickness of Al layer ( $\mu\text{g}/\text{cm}^2$ )	120	40	40.1	40	40.1
Thickness of Si ( $\text{g}/\text{cm}^2$ )	.00697	.00783	.0153	.0629	.0713
Thickness of Se (microns)	29.9	33.6	65.7	270	306
Thickness of Au layer ( $\mu\text{g}/\text{cm}^2$ )	40	40	40	40	40
Bias Voltage	13V	15V	30V	110V	80V
Active Area Diam. (mm)	14.8	17.0	19.3	21.5	25.0
Mounting Case Diam. (mm)	34.8	34.8	34.8	34.8	38.8
EG&G Model Number	TD-060- 200-25-S	TD-055- 300-34-S	TD-045- 400-86-S	TB-030- 450-225-S	TB-035- 600-300-S

an aluminum absorber and is operated in anti-coincidence with the others to veto protons with energies greater than 9 MeV. In addition, pulse height analysis is performed on pulses from the first detector in the stack to provide broad integral energy information on higher mass particles in the radiation belts.

Background noise (from stray electrons, heavy ions, or uncollimated protons) is reduced in three ways. First, passive metal shielding encases the detector stacks to eliminate side-penetrating high energy protons and electrons, and to reduce bremsstrahlung as much as possible. The high (low) stack is encased in 0.770 cm (0.876 cm) of Al, 0.254 cm (0.254 cm) of tungsten alloy, and 0.602 cm of brass (high energy head only). This shielding stops orthogonally impinging particles with energies up to 100 MeV (70 MeV) for protons and 14 MeV for electrons.

Secondly, aluminum absorbers before each detector stack reduce pulse pileup problems by stopping protons with energies less than 3.5 MeV (750 keV) before they reach the first detector.

The third form of shielding is active, in the form of guard ring detectors on the first five high energy head detectors. High energy head detector 6 (HD6) and the low energy head detectors have no rings. For high energy detectors 1 through 5 the ring is part of the same silicon wafer, but is electrically isolated from the center region. This creates a second detector outside of the acceptance angle defined by the collimation system. Figure 3 illustrates the geometry. Pulses in the detector stack which are coincident with a pulse in a ring are rejected as uncollimated particles.

The detectors in each stack are electrically isolated from chassis ground to reduce signal noise. For the high energy head, each detector is mounted in a two piece fitting, one piece of which is aluminum (the ground cup) and the other Delrin (which is an insulator.) The mechanical support holding the detectors to the chassis is done with the Delrin piece. The electrical contacts for HD2 through HD6 are ultrasonically bonded 0.7 mil diameter aluminum wire. There are two wires per contact for reliability purposes, totaling four per detector (two for center, two for the ring), except for HD6, which has no ring. HD1 is a surface barrier detector, not a SiLi, and its electrical contact is made through a surface contact. Figure 4 shows the High Energy Head detector stack, with the shielding, collimator, magnet, and HD1 removed. The face of HD2 is foremost, showing the concentric ring system and the four sonically bonded contacts.

The Low Energy Head detectors are mounted in Ortec-supplied "T-mounts", which are transmission mounts. Microdot connectors on each mount are connected to the nearby preamplifier boards by cables. The mounts of each detector are connected to signal ground, so the entire stack is isolated from chassis ground by a plastic Paralene lining evaporated onto the inside of the chassis.

Behind each detector stack is the preamplifier board mount for the head assembly. Keeping the preamplifiers close to the detectors helps reduce cable length and thus reduces noise. There is a preamplifier board for each detector, and two for the grouped high energy head rings. The boards are mounted about an aluminum support rod, and encased in an aluminum housing.

Both sensor heads are electrically isolated from the satellite ground with Delrin insulating washers inserted into the boltholes in the feet. This is done to avoid signal noise caused by chassis noise coupling into the large capacitance of the detectors.

The two sensor heads are connected to the DPU by five cable bundles (2 for the low energy head sensor, 3 for the high energy head sensor), ending in Cannon coaxial connector housings. The DPU is an aluminum box measuring 7" x 11.4" x 11.1", which houses the 12 electronics boards. The DPU then

# GUARD RING DETECTOR

## HIGH ENERGY D1 - SURFACE BARRIER

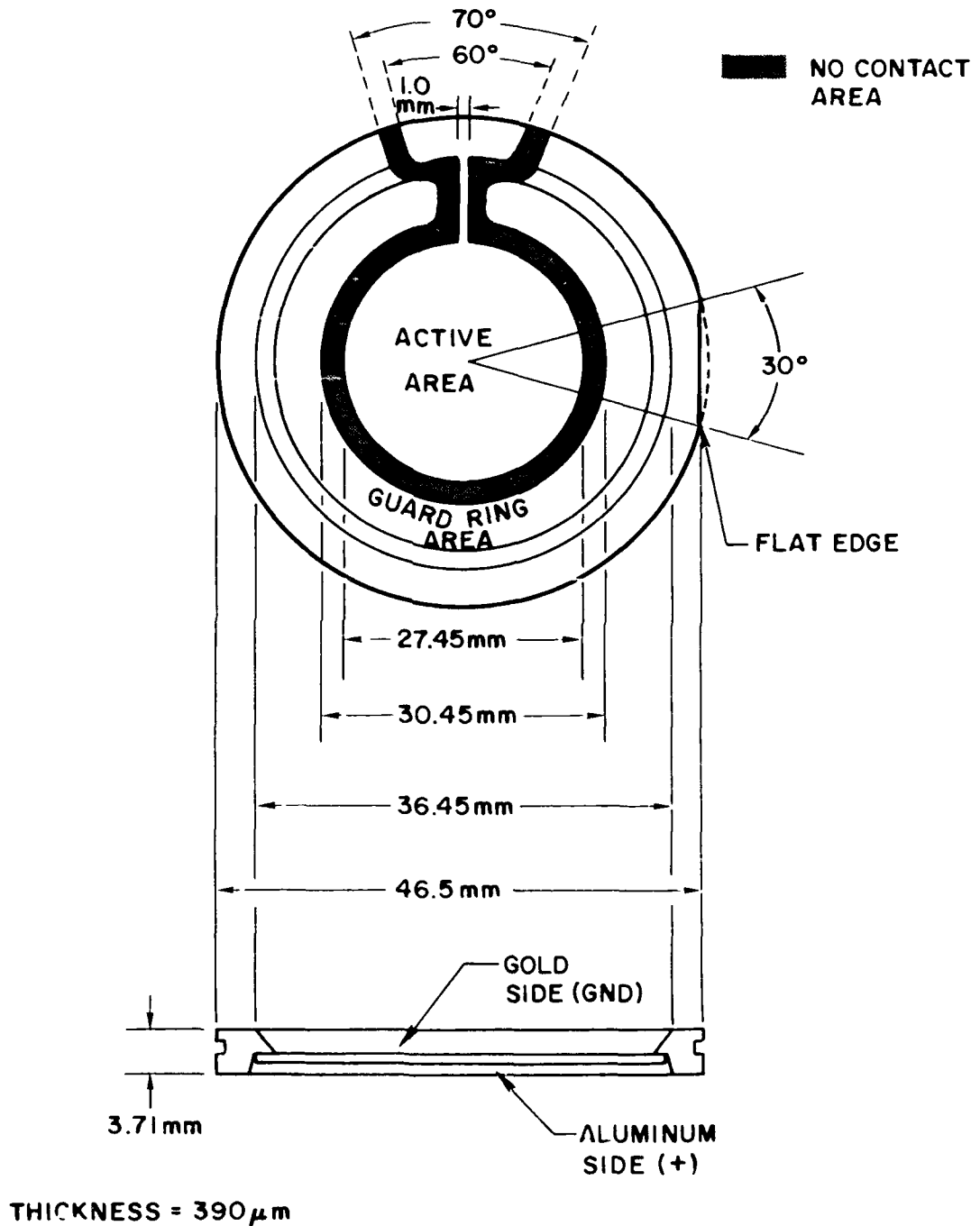


Figure 3a. Guard Rings, HD1

GUARD RING DETECTORS  
HIGH ENERGY D2-D5 Si(Li)

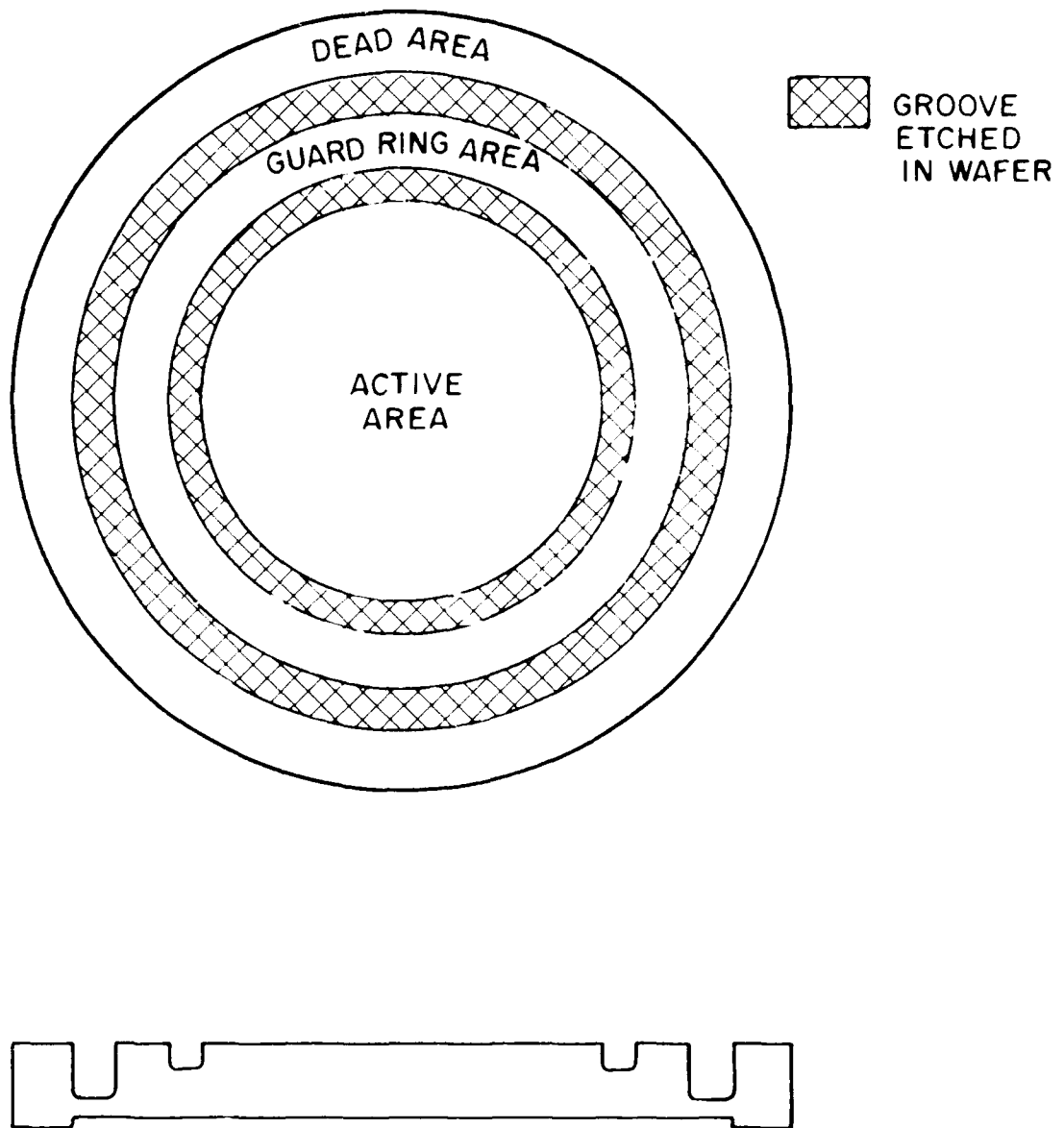


Figure 3b. Guard Rings, HD2-5

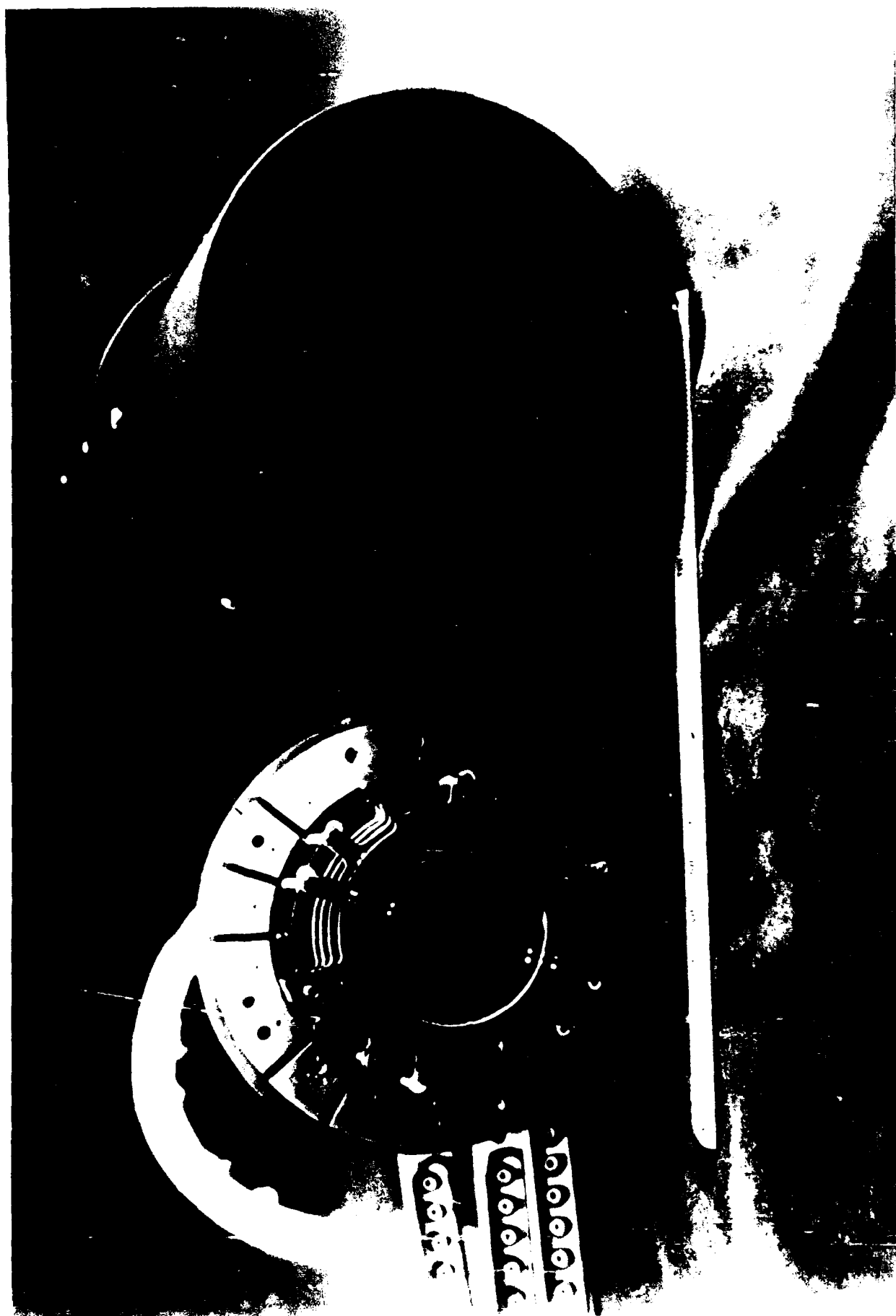


Figure 4. High Energy Head Detector Stack



attaches to the spacecraft electronics with a 50-cable bundle ending in a 50-pin Cannon connector. Figure 5 shows the three parts of the instrument mounted onto the spacecraft, with the outer spacecraft panel removed. When the panel is in place, the DPU is completely enclosed, and the two sensor heads protrude slightly through holes in the panel.

The total instrument weighs 38 lbs. It draws an average of 14 watts. The sensor heads are painted with a conductive black paint, and the DPU with a non-conductive black paint. See Table 3 for general information.

## 2.3 Logic System and Data Format

Protons of proper energy (1 - 10 MeV for the Low Energy Head, 6 - 100 MeV for the High Energy Head) impinging upon one of the sensor heads through its collimator will pass through the aluminum low energy proton absorber and lose their remaining energy in the detector stack. The amount of energy deposited in each detector and the time window within which the set of detectors is triggered are analyzed by the logic system. If the system approves the validity of the event, it then determines the incident energy of the original proton and causes a count to be registered in the proper channel. Table 1 is the logic table which shows, for a given incident energy proton, how much energy is deposited in each detector. The incident energies listed form the boundaries of the energy bins from which the proton spectrum is deduced. Table 1a is for the HEH, Table 1b for the LEH, and Table 1c for the heavy ions in LD1.<sup>15,20,21</sup>

These energy deposition tables are based on range energy relations for protons passing through silicon, aluminum, and gold.<sup>15</sup> For a particle stopping in a slab of material, the energy deposited in the slab is linear, and approximately equal to the incident energy of the particle. Once the particle has sufficient incident energy to pass through the slab, the deposited energy drops off sharply. Thus a graph of energy deposited in a slab vs. incident energy (see Figure 6a) has a linear rise followed by a sharp decline, with the peak at the maximum incident energy that can be stopped by the slab. Figure 6b (6c) is a plot of the deposited energy (energy deposited in detector active area) vs. incident energy (particle energy outside the sensor head) for the High (Low) Energy Head detectors. Figure 6d is a plot of heavy ion depositions in LD1. These range energy relationships are used to construct the logic tables shown in Table 1.<sup>15,20,21</sup>

There are two steps to the logical analysis described above. In the first step, the system checks to see that all the triggered detectors were turned on within a fixed time window (0.5  $\mu$ sec for the HEH, 2.0  $\mu$ sec for the LEH). In the second step, the system measures the energy deposited in each detector to determine in which, if any, channel the particle should be recorded. For instance, if a proton in the HEH leaves 2.6 MeV in D1, 4 MeV in D2, 11 MeV in D3 (see Table 1a), and nothing in D4, D5, D6, or the rings, all within a 0.5  $\mu$ sec time window, it will be recorded as a channel 8 HEH count, that is, a proton with incident energy between 18.08 MeV and 24.715 MeV. Most channels require either a double or a triple coincidence.

---

15. Janni, J.F. (1982) Proton range-energy tables, 1 keV - 10 GeV, *Atomic Data And Nuclear Data Tables* **27**:4/6.

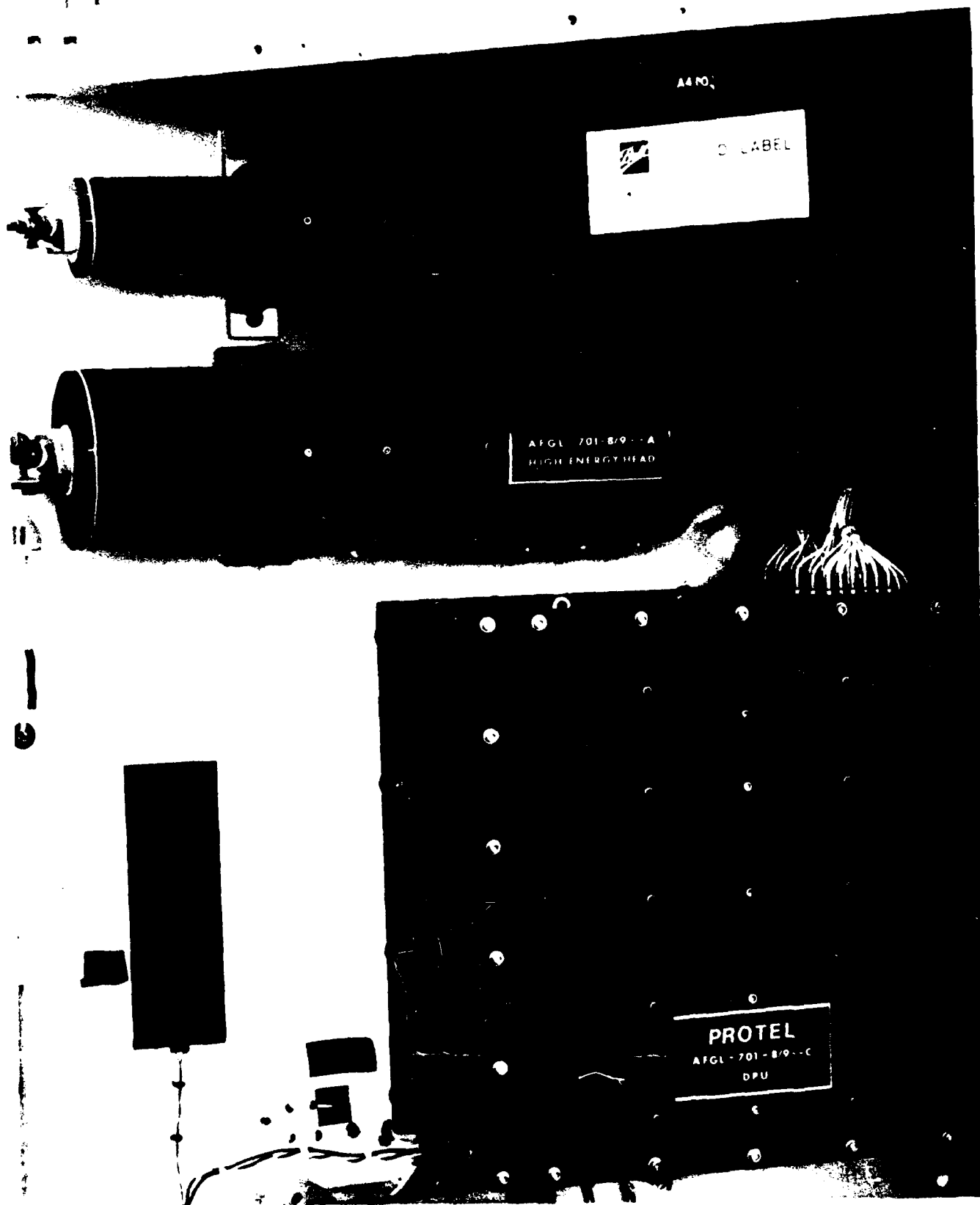


Figure 5. PROTEL Mounted on Spacecraft

Table 3. General Information

POWER	14 W; 500 mA	
WEIGHT	HEH	15.8 lbs.
	LEH	7.0 lbs.
	<u>DPU</u>	<u>15.6 lbs.</u>
	TOTAL	38.45 lbs.
SIZE	HEH	12.7" long by 4" diameter
	LEH	13.3" long by 2.4" diameter
	DPU	7" by 11.4" by 11.1"
OPERATING TEMPERATURE RANGE	-10°C to +28°C (sensor heads)	
ENERGY RANGE MEASURED	1 to 100 MeV protons	
GEOMETRIC FACTORS	HEH	0.119 cm <sup>2</sup> -ster
	LEH	0.012 cm <sup>2</sup> -ster
	(for isotropic flux)	

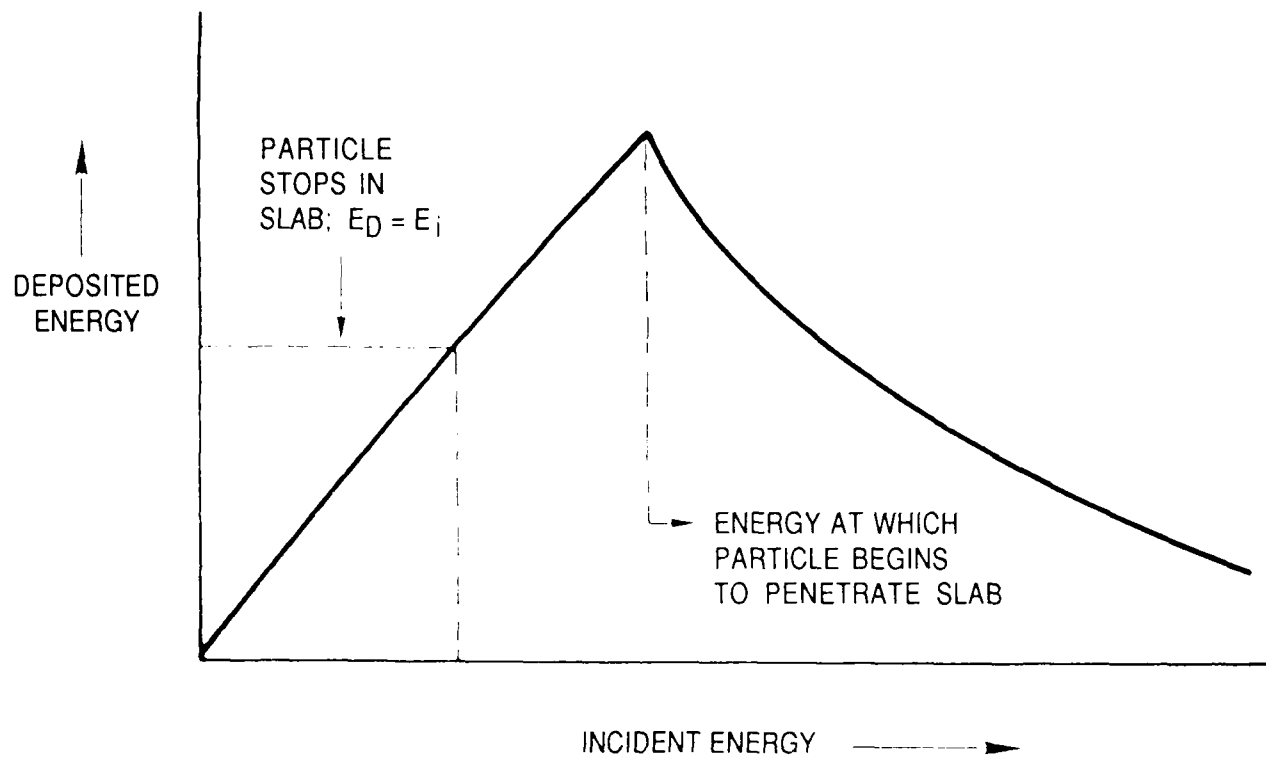


Figure 6a. Deposited vs. Incident Energy Curves. Graph of energy deposited in a Silicon Slab vs. Incident Proton Energy

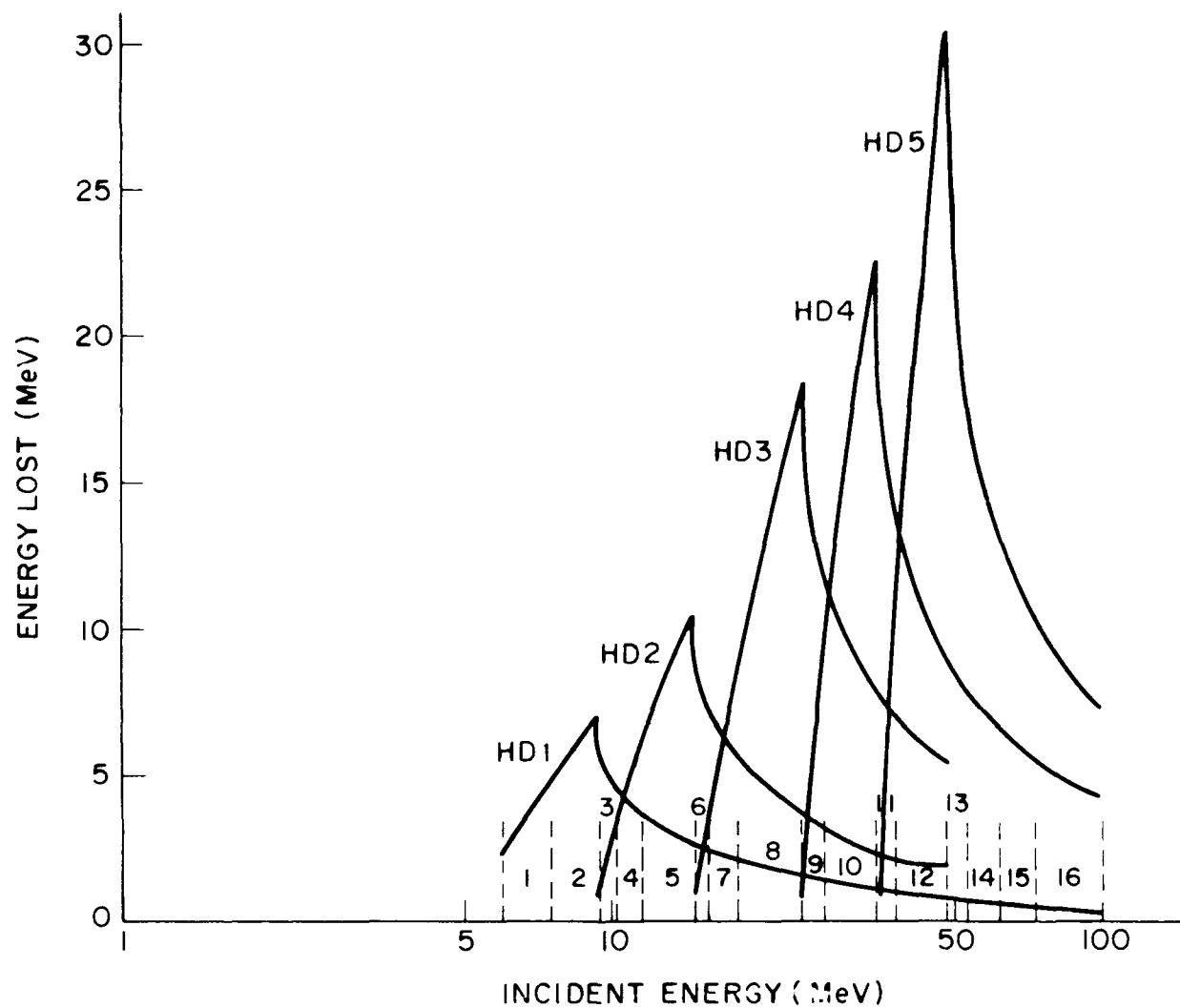


Figure 6b. Deposited vs. Incident Energy Curves. Graph of energy deposited in each of the detectors in the High Energy Stack vs. Incident Particle Energy

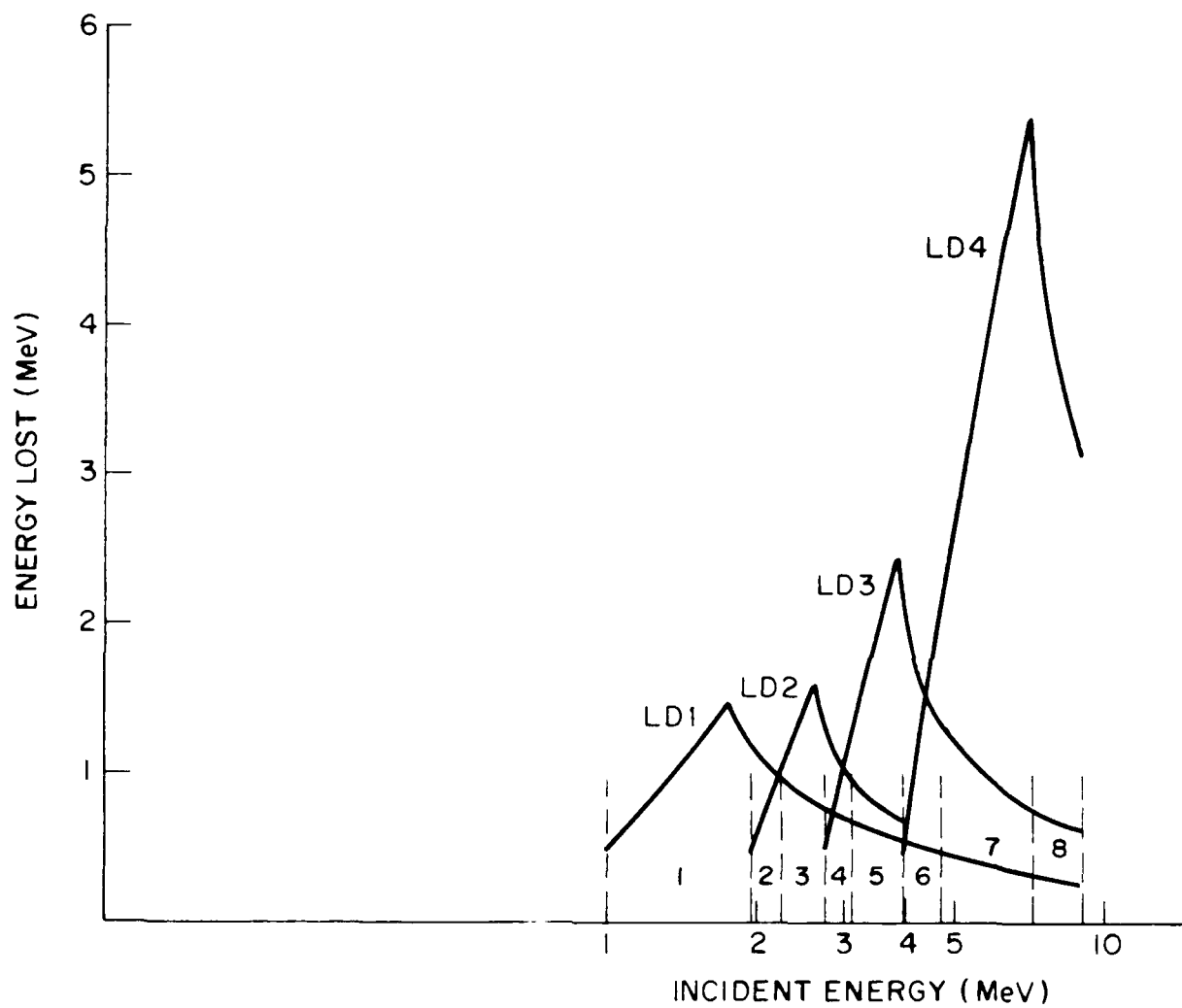


Figure 6c. Deposited vs. Incident Energy Curves. Same as 5b, but for the Low Energy Head

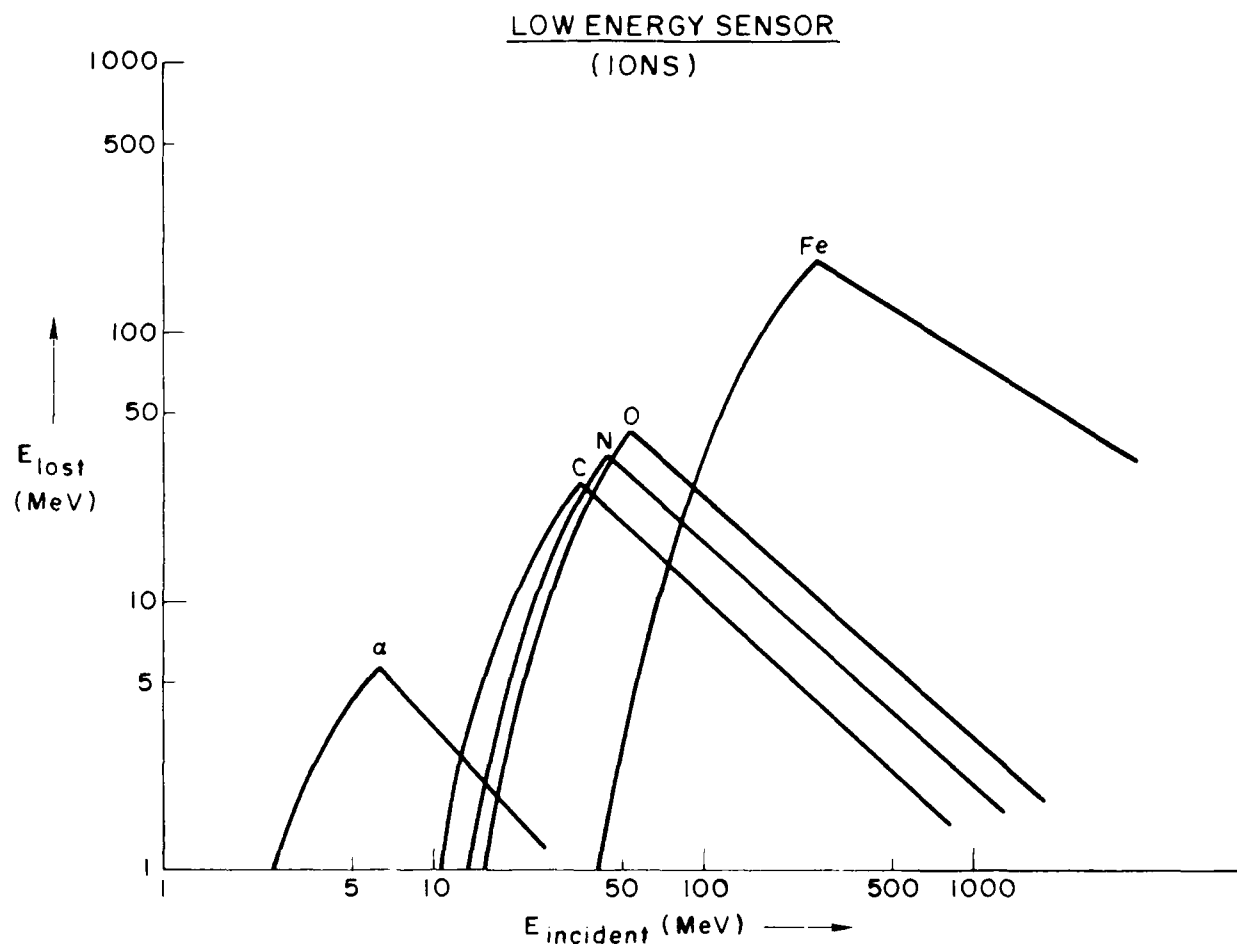


Figure 6d. Deposited vs. Incident Energy Curves. Same as 5b, but for the Low Energy Head Heavy Ions

There are many circumstances under which the coincidental triggering of several detectors will not yield a valid count. If the detectors are not triggered within the time window, or if one of the ring detectors is triggered within that same time window, or if, in the above example, D4, D5, or D6 is triggered within that window, the event is not recorded as a count. In addition, if the timing is correct, but the energy deposited in any one of the detectors is not within the specified ranges, the event is not counted. That is to say, if the channel 8 particle described above for some reason (long path length in the detector, a nuclear star interaction, detector noise) deposited 5.5 MeV instead of 4 MeV in D2, then D2 would call the particle a channel 7 proton, disagreeing with D1 and D3, and the event would be not be counted in any channel.

The vetoing power of any of the detectors can be turned off. If one of the detectors becomes noisy, it can be effectively removed from the logic system by a command which causes the detector to be ignored by the logic, with respect to both timing and energy deposition. If it is necessary to look at one detector at a time, for instance in the calibration routine or when checking the gains, all of the other detectors can be made transparent in this way, and any logic decisions are performed by the one remaining detector.

In addition to the proton spectra measurements, PROTEL also has the capability of crudely counting heavy ion fluxes, using the first detector of the LEH, LD1. This detector is attached to an additional amplifier/PHA circuit which is triggered by pulses in LD1 which exceed 6 MeV. Table 1c lists the threshold levels, in energy deposited, for each of the five heavy ion channels. Note that these channels, unlike the proton channels, are identified by the energy deposited, not incident energy. This is because the incident energies causing a particular deposited energy will vary depending on particle type. Table 1c also lists some sample incident energies for several particle species.

The data returned from PROTEL are formatted into two data displays, the science data (Figure 7) and the housekeeping data (Figure 8). The science data screen shows the raw counts and valid channel counts for both head assemblies and the heavy ion channels. The housekeeping data display monitors all the analog values (temperatures, voltages) and the command system status.

The science data display, shown in Figure 7, is divided into five columns. The first column shows the analyzed counts accumulated by the pulse height and logic system in each channel, 1 through 16, for the high energy head. The incident energies corresponding to these channel numbers are listed in Table 1a. The second column, also for the high energy head, lists raw counts and semi-analyzed counts. The counts listed next to D1 - D6, and DR, are the raw counts in each detector and in the rings, that is, the number of pulses in each detector that were sufficient to trigger the lowest energy threshold for that detector, independent of the size of the pulse or whether it was coincident with a pulse in another detector. The counts in the upper half of the column, next to labels such as DxyA, are the number of events which triggered detector x and detector y, but not detector 6, within a certain time window, but independent of the size of the pulses.

The next three columns are for the Low Energy Head. Column three is similar to column one, showing the counts for valid events accumulated in each channel. Column four is like column two, listing raw counts and timing-analyzed counts. The last column lists the valid counts accumulated in the heavy ion channels for LD1. The science data display is fully updated four times during every major frame, so a full spectrum is returned once a second.



FO920 DISK1  
ACCUMULATED TELEMETRY DATA

Data for 9-AUG-86 10:49:17  
Valid sets accumulated = 120  
Beam Configuration: 0 DEG

92.0 MEV 3500 CTS/S

HEA		HED		LEA		LED		HI	
1	294.	D1A	170544.	1	0.	D1A	0.	1	0.
2	279.	D12A	150832.	2	0.	D12A	0.	2	0.
3	62.	D123A	120376.	3	0.	D13A	0.	3	0.
4	113.	D134A	127376.	4	0.	D134A	0.	4	0.
5	431.	D145A	120376.	5	0.	D5	0.	5	0.
6	95.	D6	1004416.	6	0.	D1	0.	6	0.
7	363.	Dr	20402.	7	0.	D2	0.	7	0.
8	830.	D1	170576.	8	0.	D3	0.	8	0.
9	285.	D2	252752.			D4	0.	9	0.
10	2026.	D3	357632.					10	0.
11	579.	D4	316416.						
12	8422.	D5	378688.						
13	1867.								
14	6603.								
15	4522.								
16	24438.								

Figure 7. Science Data Display. Science data display for accumulated proton accelerator beam data from the High Energy Head sensor calibration. The Low Energy Head sensor was not exposed to the beam at the same time. This sample is from the Harvard calibration, at 92 MeV, and it shows 480 seconds of accumulated telemetry data.

# HOUSEKEEPING DATA

Analog data taken 9 AUG 86, 10:49:17

Bilevel data taken 9 AUG 86, 10:49:04

Beam Configuration: 0 DEG

92.0 MEV

3500 CTS/S

Experiment Power is ON

H.E. AMP TEMP	=	26.6	C	Ch01	H.E. DET 1	=	0	COMMAND 1	=	0
L.E. AMP TEMP	=	25.0	C	Ch02	H.E. DET 2	=	0	COMMAND 2	=	0
DC-DC TEMP	=	49.4	C	Ch03	H.E. DET 3	=	0	COMMAND 3	=	0
H.E. up TEMP	=	31.6	C	Ch04	H.E. DET 4	=	0	COMMAND 4	=	0
+10 V SUPPLY	=	9.64	V	Ch05	H.E. DET 5	=	0	H.E. MEM SW UL	=	0
+15 V SUPPLY	=	-14.77	V	Ch06	H.E. DET 6	=	0	H.E. MEM SW UR	=	0
-15 V SUPPLY	=	14.86	V	Ch07	H.E. RINGS	=	0	H.E. MEM SW LL	=	0
+5 V SUPPLY	=	4.90	V	Ch08	H.E. SUM	=	0	H.E. MEM SW LR	=	0
H.E. DET 1 BIAS	=	101.6	V	Ch09	L.E. DET 1	=	0	L.E. MEM SW UL	=	0
H.E. DET 2 BIAS	=	174.0	V	Ch10	L.E. DET 2	=	0	L.E. MEM SW UR	=	0
H.E. DET 4 BIAS	=	392.9	V	Ch11	L.E. DET 3	=	0	L.E. MEM SW LL	=	0
H.E. DET 6 BIAS	=	396.7	V	Ch12	L.E. DET 4	=	0	L.E. MEM SW LR	=	0
L.E. DET 1 BIAS	=	14.34	V	Ch13	L.E. DET 5	=	0	CAL.ENABLE UL	=	0
L.E. DET 3 BIAS	=	33.83	V	Ch14	L.E. SUM	=	0	CAL.ENABLE UR	=	0
L.E. DET 5 BIAS	=	75.25	V	Ch15	CELL 2,4	=	0	CAL.ENABLE LL	=	0
L.E. up TEMP	=	26.8	C	Ch16	CELL 2,7	=	0	CAL.ENABLE LR	=	0

Figure 8. Housekeeping Data Display. Housekeeping data for normal operation (all detectors actively participating in logic analysis). This sample corresponds to the science data sample in Figure 7.

Figure 8 is a sample of the housekeeping data display. The first column monitors all the analog data, such as temperatures and voltages. The other two columns list the command matrix status. The command system status is fully updated every four major frames (sixteen seconds).

The specific meanings of the information monitored in the housekeeping data display are as follows. HE and LE AMP TEMP are the temperatures, in degrees Celsius, recorded by thermistors on the preamplifier assemblies attached to the backs of the sensor heads. DC-DC TEMP is the temperature of the converter boards in the DPU. HE and LE uP TEMP are the temperatures on the high energy and low energy microprocessor boards. The power supply voltage monitors are self-explanatory. HE and LE DET # BIAS monitors track the overbias voltages on some of the detectors. Their nominal values range from 14V (for LD1) to 400V (for HD4&6).

In the second column, the HE DET #'s and LE DET #'s, and HE RINGS, show the command cell status for each detector. If the detector has been made transparent, this should read "1". Under normal operation, all should read "0". HE and LE SUM show the status of the summing logic, which is invisible to the user. Cell 2,4 and cell 2,7 are unused commands.

The third column shows the status of COMMAND 1-4, which, when changed together as a group of four, change the command system path to a redundant one in case of a failure. The different permutations of the four commands result in  $2^4$ , or 16, possible redundant command system paths. Next are the quad command memory switches HEMEMSWxx and LEMEMSWxx, which change the memory systems to redundant ones in case of a failure. Also shown is whether the calibration system has been enabled, CALENABLExx. If the calibration system is sending pulses into the PHAs, all four CALENABLE cells will read "1".

## **2.4 Electronics, Commands, and Telemetry**

### **2.4.1 ELECTRONICS DESIGN**

The data processing unit (DPU) controls the coincidence logic and formats the data for transmittal to the spacecraft telemetry system. Figure 9 is a block diagram of the basic components and interconnections for the instrument. The low energy sensor electronics are similar in design, but with one fewer detector and no ring detectors. The main components of the system are the front end preamplifiers, buffer preamplifiers, coincidence and anti-coincidence logic system, pulse height analyzers and associated decoding logic, accumulator latches, a data formatting microprocessor, a command system, and a power supply system. The preamplifiers are commercial low-power hybrid integrated circuits, configured as a charge amplifier followed by a single pole shaping amplifier with an approximate gain of 10. The charge amplifiers are located on the back of the detector housing in close proximity to the silicon detectors, reducing the cable and stray capacitance at the inputs and lowering the sensitivity to radiated EMI from the instrument and spacecraft systems. The buffer amplifiers are located in the data processing unit. These permit the gain adjustments required to accommodate the different energy ranges of each detector. Thicker detectors stop more of a particle's energy, so their output pulses will, in general, be larger than those of thin detectors. The buffer amplifiers adjust for these different ranges so that the pulses vary over the same range

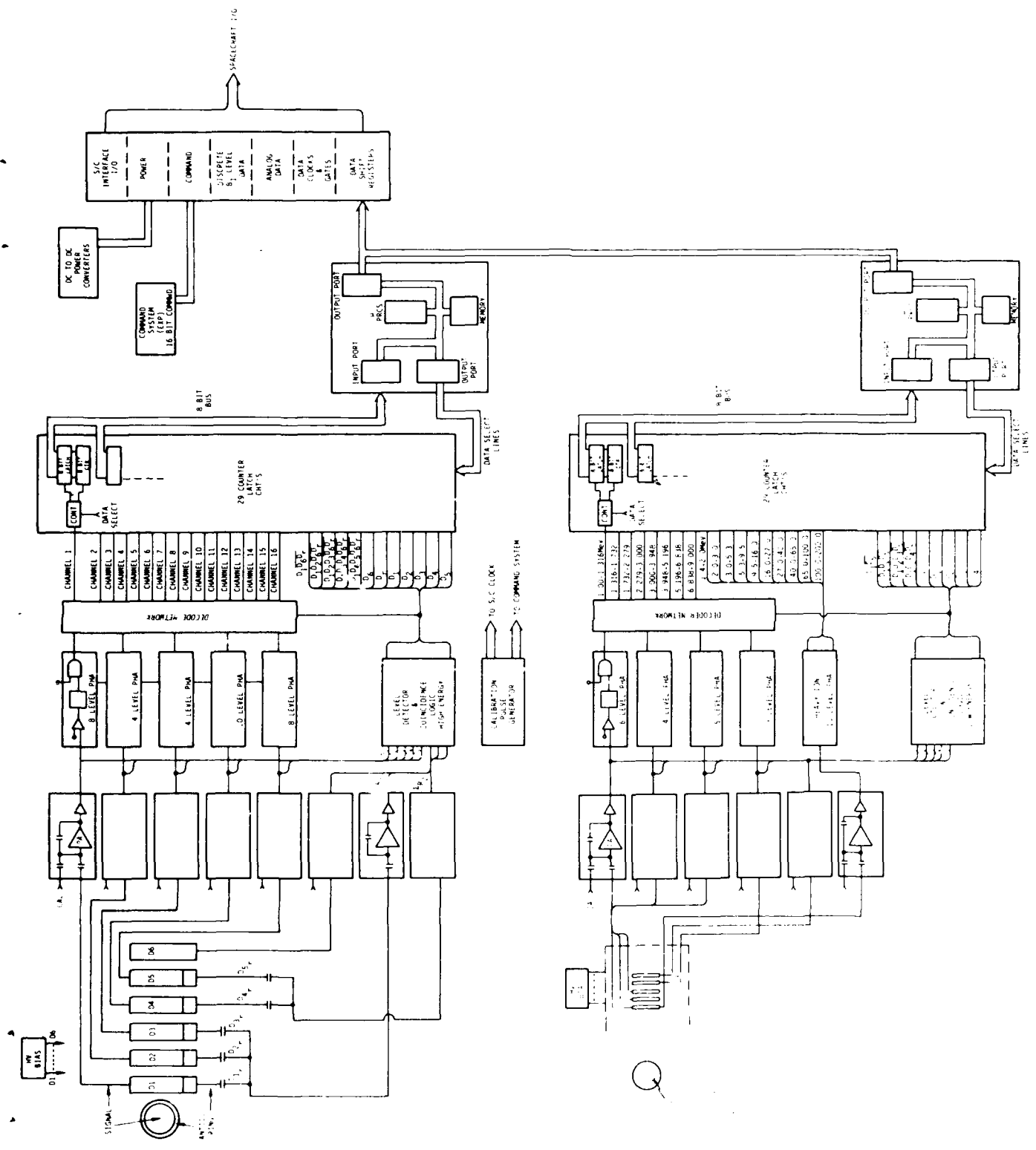


Figure 9. Block Diagram of DPU Electronics

(0 to 5.5 V, approximately) for each detector. They also establish a low source impedance for the input to the logic and pulse height analysis circuitry.

The coincidence logic circuitry controls the pulse height thresholds, the detector coincidence scheme, and the active background rejection. Fast (~30 ns) level comparators are used to measure the lowest energy level pulse for each detector. If the comparators of different detectors are triggered within a coincidence window of 0.5 microsecond (2.0 microseconds for low energy system), the logic system then analyzes the pulse sizes to see if a valid event occurred. Active shielding for background rejection is performed logically using the outputs from the sixth detector and the rings in the high energy head and from the fifth detector in the LEH. If one of the shielding detectors' comparators triggers within the coincidence window mentioned above, the event is not counted.

Each of the coincidence detectors has a stacked comparator pulse height analyzer (PHA). There are nine PHAs in all, five for the high energy head and four for the low. The tripping of the threshold settings of these comparators establishes the energy lost in a given detector. The output of all the PHAs is then logically compared to check for a valid coincidence count.

A ripple counter accumulates valid counts and stores them in the microprocessor memory system. The microprocessor regularly polls these counters, which share a common bus, and stores the value of each counter in memory, then clearing the counter. This determines one of the fundamental counting rate limits on the system to be < 255 counts per microprocessor polling period (1 msec). This memory system also formats the stored data and includes the interface required to transmit the data to the spacecraft telemetry system.

## 2.4.2 COMMANDS AND TELEMETRY

PROTEL is controlled by the experiment command system. Commands are sent to the instrument via a spacecraft supplied sixteen bit serial digital command word. Verification of commands and instrument status is done using the PROTEL housekeeping telemetry words, which consist of 17 analog outputs and 9 bilevel outputs. In addition, there are 55 science data telemetry words which are used to carry the measured spectra.

Table 4 lists the 32 different commands that can be used to alter the status of the instrument. Each of these commands corresponds to one of the elements in the second two columns of the housekeeping data display. (See Figure 8) COM1-COM4 are used together as a quad command which changes the path of the command system to a redundant path in case of a failure. HEMEMA-HEMEMD and LEMEMA-LEMEMB are quad commands used to switch either the high energy head system or the low energy head system, respectively, to their redundant memory circuits, in case of primary circuit failure.

HED1-HED6, HEDRING, and LED1-LED6 are single commands used to make a particular detector circuit transparent to the logic. For example, if the low energy head detector #1, LD1, becomes excessively noisy due to radiation damage, the command LED1=1 will be sent, and the logic system will bypass LD1 in its decisions concerning the changing of raw counts into valid events. Also, these detector commands are used in groups during the calibration sequences, turning all but one detector transparent at a time, so that the logic system only uses the response from one detector. These sequences will be discussed in more detail in the next section.

Table 4. Command Matrix Cells and Mnemonics

The Mnemonic is the name used to refer to the command; The Cell is the location in the command matrix; The Command String is the bit sequence to send the command. The "t's" in the command string are determined by the status of the command matrix at the time the command is sent. The "x's" have no bearing on the command, and are usually set to 0. The commands are sent up as 16 bit serial digital command words. Their status is read out in the telemetry using analog A236 and bilevels B294-304.

Mnemonic	Cell	Command				Function
COM1	C11	xxxx	ttt1	0000	0001	command system configuration switch 1
COM2	C33	xxxx	t1tt	0000	0100	switch 2
COM3	C13	xxxx	ttt1	0000	0100	switch 3
COM4	C31	xxxx	t1tt	0000	0001	switch 4
HEMEM A	C15	xxxx	ttt1	0001	0000	high energy system alternate memory, switch a
HEMEM B	C26	tt1t	xxxx	0010	0000	switch b
HEMEM C	C37	xxxx	t1tt	0100	0000	switch c
HEMAM D	C48	1ttt	xxxx	1000	0000	switch d
LEMEM A	C12	ttt1	xxxx	0000	0010	low energy system alternate memory, switch a
LEMEM B	C23	xxxx	tt1t	0000	0100	switch b
LEMEM C	C34	t1tt	xxxx	0000	1000	switch c
LEMEM D	C45	xxxx	1ttt	0001	0000	switch d
HED 1	C18	ttt1	xxxx	1000	0000	turn on/off HED 1
HED 2	C32	t1tt	xxxx	0000	0010	turn on/off HED 2
HED 3	C21	xxxx	tt1t	0000	0001	turn on/off HED 3
HED 4	C17	xxxx	ttt1	0100	0000	turn on/off HED 4
HED 5	C43	xxxx	1ttt	0000	0100	turn on/off HED 5
HED 6	C22	tt1t	xxxx	0000	0010	turn on/off HED 6
HERING	C41	xxxx	1ttt	0000	0001	turn on/off HE rings
HESUM	C44	1ttt	xxxx	0000	1000	turn on/off HE summation counter
LED 1	C38	t1tt	xxxx	1000	0000	turn on/off LED 1
LED 2	C28	tt1t	xxxx	1000	0000	turn on/off LED 2
LED 3	C42	1ttt	xxxx	0000	0010	turn on/off LED 3
LED 4	C16	ttt1	xxxx	0010	0000	turn on/off LED 4
LED 5	C35	xxxx	t1tt	0001	0000	turn on/off LED 5
LESUM	C46	1ttt	xxxx	0010	0000	turn on/off LE summation counter
CALEN A	C14	ttt1	xxxx	0000	1000	calibration system enable, switch a
CALEN B	C25	xxxx	tt1t	0001	0000	switch b
CALEN C	C36	t1tt	xxxx	0010	0000	switch c
CALEN D	C47	xxxx	1ttt	0100	0000	switch d
unused	C24	tt1t	xxxx	0000	1000	-
unused	C27	xxxx	tt1t	0100	0000	-

Continuing down Table 4, commands HESUM and LESUM change the summation counter for the high or low energy head system, respectively. This change is transparent to the user. Commands CALENA-CALEND are a quad command. When all four are set = 1, the calibration system in the DPU is enabled. The calibration system then sends ramps of pulses to the preamplifiers, to check the circuitry from the preamps through the DPU. Finally, there are two unused commands. The housekeeping data display monitors the status of each of the 32 commands, listing each mnemonic and whether it is set to "0" or to "1".

To change the status of the instrument by sending one of the above commands, one uses a sixteen bit command word supplied by the spacecraft. The command word is encoded from a four by eight matrix of static on-off command elements, called cells, with each of the commandable functions listed above controlled by one or more of these cells. The command cell matrix is then:

C11	C12	C13	C14	C15	C16	C17	C18
C21	C22	C23	C24	C25	C26	C27	C28
C31	C32	C33	C34	C35	C36	C37	C38
C41	C42	C43	C44	C45	C46	C47	C48

where each element is equivalent to one of the command mnemonics in Table 4. The more critical functions utilize several redundant elements (quad commands). Table 4 includes a listing of which command matrix cell controls which function.

For example, if the LD1 detector were to be made transparent as described above, the command with mnemonic LED1=1 would be sent by changing the status of command cell number C38 from a "0" to a "1". Under normal operation, all of the command cell elements are set to "0". If, for example, LD1 is made transparent, the matrix would be all zeros except for C38, which would be a "1", and the matrix representation of the status of the instrument would look like:

0	0	0	0	0	0	0	0
0	0	0	0	0	0	0	0
0	0	0	0	0	0	0	1
0	0	0	0	0	0	0	0

To send commands to alter this matrix, and thus to alter the state of the instrument, the minimum unit of change is a full column of four cells. This means that to change one element of the matrix, it is necessary to know the values of the other three elements in the same column, because they must be reset to their same values, since the matrix can only be manipulated in groups of four-cell changes in a given column. To change a row of the matrix, and thus send a command, one sends a sixteen bit spacecraft serial digit command word in the following format:

15 14 13 12 11 10 9 8 7 6 5 4 3 2 1 0  
 <---- bit number---

Bits 0 through 7 select which of the eight columns is to be changed. If column 4 is to be changed, the bit configuration, from bit 7 to bit 0, would be 00001000. Only one column is changed at a time.

The data which are to be entered into the command matrix column are sent in the last eight bits. Data for odd numbered columns are sent in bits 11 through 8, and for even numbered columns in bits 15 through 12, with row 1 data for odd columns in bit 8, and row one data for even columns in bit 12.

As an example, let the command matrix status be as shown above, with all cells zero except C38, that is, normal operation except that LD1 has been made transparent to the logic. Now let us say that HD1 has also become excessively noisy for some reason and we wish to remove it from the logic. Then we will want to set HED1=1, which means we need to set matrix element C18 to "1". We will be sending a sixteen bit serial digital command word to change column number 8, so bits 7-0 in our word will be:

1 0 0 0 0 0 0 0

Since column number eight is an even column, we will put the data for the newly changed column in bits 15-12, which will be:

0 1 0 1

Bit 12 corresponds to cell C18, which is the one we are changing here to a "1". Bit 13 is cell C28, which we are resetting to "0". Bit 14 is cell C38, which we are resetting to "1" (it was set to a one in the previous example, where LD1 was made transparent), and bit 15 is cell C48, reset to "0". The remaining four bits in the word concern the changing of odd numbered rows and have no meaning in this word, so we can just set them to 0 (or to 1, it makes no difference); then our total command word is as follows, starting with bit 15:

0 1 0 1      0 0 0 0      1 0 0 0      0 0 0 0

Sending of the command, then, is done with a spacecraft supplied 16 bit serial digital command word. Verification that the proper command was sent and received is done by using a combination of the eight PROTEL bilevel lines and one of the PROTEL analog lines. The eight bilevels correspond to the eight columns of the matrix. The one analog line has four distinct voltage levels which correspond to the four rows of the matrix. The nominal voltage-to-row conversion on the analog line is:

row 1	:	0.0V
row 2	:	1.5V
row 3	:	3.0V
row 4	:	4.5V

For example, if bilevel 7 is a 1 when the analog data line is at 3V, then the status of command cell C37 is "1". The instrument will step through all four voltages over four major frames.

Most of the above explanation concerns details that are relatively invisible to the user. The telemetry stream from the instrument is formatted into two screens as soon as it is received from the spacecraft. The two screen formats, the science data and the housekeeping data, were described previously. (See Figures 7 and 8.) The science data format displays the counts per second that have been processed through the DPU. The housekeeping data format lists the "1" or "0" status of each of the 32 command cells described above, but listed by their corresponding mnemonics, not by their matrix cell numbers. The housekeeping data also lists the data from the other 15 analog lines, which monitor various temperatures and voltages within the PROTEL instrument.

The housekeeping data are constructed from the 8 bit commutated analog data and the bilevel outputs. Both of these are located in a subcom (see Figure 10) in the spacecraft telemetry stream. PROTEL has 17 analog outputs (A221 - A237 are the CRRES spacecraft designations) and 9 bilevel outputs (B29 - B30 are the CRRES spacecraft designations.) The analog outputs are listed in Table 5.



# GTO FORMAT

Downlink Rate Major Frame Minor Frame

1.0 KBPS 65.536 Sec 2.048 Sec  
 \*\* 16.0 KBPS 4.096 Sec .128 Sec \*\* Normal Test Rate  
 64.0 KBPS 1.024 Sec .032 Sec  
 256.0 KBPS 0.256 Sec .008 Sec

	0	1	2	3	4	5	6	7	8	9	10	11	12	13	14	15	16	17	18	19	20	21	22	23	24	25	26	27	28	29	30	31
0	S	S	S	S	S	S	S	S	S	S	S	S	S	S	S	S	S	S	S	S	S	S	S	S	S	S	S	S	S	A	B	FC
	32	32	32	32	32	33	36	36	33	33	36	36	38	39	36	36	34	38	34	41	30	34	40	35	34	42	34	35	34	295	35	
32	S	S	S	S	S	S	S	S	S	S	S	S	S	S	S	S	S	S	S	S	S	S	S	S	S	S	S	S	S	S/O	S/O	S/C
	31	31	31	31	33	33	36	36	33	38	36	36	38	39	36	36	34	38	34	41	30	34	40	35	34	42	34	35	34	0	1	2
64	S	S	S	S	S	S	S	S	S	S	S	S	S	S	S	S	S	S	S	S	S	S	S	S	S	S	S	S	S	S/O	S/O	S/C
	32	32	32	32	32	33	36	36	33	33	36	36	38	39	36	36	34	38	34	41	30	34	40	35	34	42	34	27	34	3	4	5
96	S	S	S	S	S	S	S	S	S/O	S	S	S	S	S	S	S	S	S	S	S	S	S	S	S	S	S	S	S	S	S/O	S/O	S/C
	31	31	31	31	33	33	36	36	33	15	36	36	38	39	36	36	34	38	34	41	30	34	40	35	34	42	34	27	38			VTCW
128	S	S	S	S	S	S	S	S	S	S	A	A	S	S	A	A	S	S	S	S	S	S	S	S	S	S	S	S	S	S/O	S/O	S/C
	32	32	32	32	32	33	36	36	33	33	246	247	38	39	248	249	34	38	34	41	30	34	40	35	34	42	34	27	42	6	7	8
160	S	S	S	S	S	S	S	S	S/O	S	A	A	S	S	A	A	S	S	S	S	S	S	S	S	S	S	S	S	S	S/O	S/O	S/C
	31	31	31	31	33	33	36	36	33	16	250	251	38	39	252	253	34	38	34	41	30	34	40	35	34	42	34	27	42	9	10	11
192	S	S	S	S	S	S	S	S	S	S	A	A	S	S	A	A	S	S	S	S	S	S	S	S	S	S	S	S	S	S/O	S/O	S/C
	32	32	32	32	32	33	36	36	33	33	254	255	38	39	256	257	34	38	34	41	30	34	40	35	34	42	34	27	42	12	13	14
224	S	S	S	S	S	S	S	S	S	S	A	A	S	S	S/O	S/C	S	S	S	S	S	S	S	S	S	S	S	S	S	S/O	S/O	SYNC.
	31	31	31	31	33	33	36	36	33	38	258	259	38	41	18	19	34	38	34	41	30	34	30	35	34	42	34	17	42			

A = Analog Word  
 B = Bilevel Word  
 S = Serial-Digital Word  
 FC = Frame Counter  
 Sync. = Synchronization Word  
 S/C = Subcom

Figure 10. Spacecraft Telemetry Stream - One Minor Frame. The telemetry stream from the spacecraft for one minor frame. The words and subcoms allocated to PROTEL are highlighted. There are 32 minor frames in one major frame. The science data display is constructed from the science data words; it takes eight minor frames to completely update the science data. The housekeeping data is constructed from the analog signals and the bilevels, which are located in the subcoms. It takes four major frames, or 128 minor frames, to completely update the housekeeping data. The PROTEL science data words are located in the blocks labelled S-35. The PROTEL analogs are located in subcom S/C-11, and come up in minor frames 15 through 31. Their spacecraft designation is A221 through A237. The PROTEL bilevels are located in minor frames 19 and 20 of subcom S/C-14. Their spacecraft designations are B294 through B304.

Table 5. Analog Signals and Mnemonics

The telemetry designations are the spacecraft names for the analogs. They are located, in Figure 9, in S/C-11.		
Mnemonic	Telemetry Designation	Function
H.E. AMP TEMP	A221	HEH Preamplifier Temperature
L.E. AMP TEMP	A222	LEH Preamplifier Temperature
DC-DC TEMP	A223	DC-DC Converter Temperature
H.E. $\mu$ P TEMP	A224	HEH Microprocessor Temperature
+10 V SUPPLY	A225	Power Supply
+15 V SUPPLY	A226	"
-15 V SUPPLY	A227	"
+5 V SUPPLY	A228	"
H.E. DET1 BIAS	A229	Detector Bias Voltage
H.E. DET2 BIAS	A230	"
H.E. DET4 BIAS	A231	"
H.E. DET6 BIAS	A232	"
L.E. DET1 BIAS	A233	"
L.E. DET3 BIAS	A234	"
L.E. DET5 BIAS	A235	"
	A236	Used for command system
L.E. $\mu$ P TEMP	A237	LEH Microprocessor Temperature

They are updated once per major frame. The housekeeping display is shown in Figure 8. It is completely updated once every four major frames, on a rolling basis.

The PROTEL science data words have 11 bits and are broken up to conform to the 8 bit word satellite telemetry format. Construction of the 11 bit science data words from the 8 bit minor frame telemetry words is shown in Figure 11. It is repeatable for each minor frame. The satellite telemetry stream for one minor frame, with the applicable words for PROTEL highlighted, is shown in Figure 10. The 11 bits of the PROTEL science data word correspond to an 11 bit logarithmically formatted number:

Xxxx XXXXXXX (X is most significant bit)  
exponent mantissa

Each 11 bit word is converted to base 10 and displayed as a science data "count" in the right hand sides of the columns of the science data format shown in Figures 7 and 12. The left hand sides of the columns remain constant throughout the display.

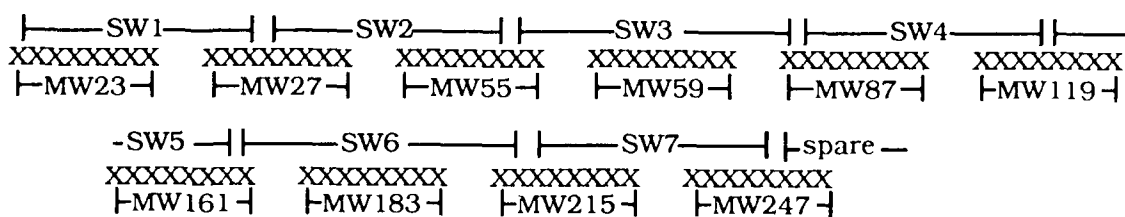
In a set of 8 satellite minor frames, the first seven each include 7 PROTEL science data words and 3 PROTEL spare bits, and the eighth has 6 PROTEL words and 14 spare bits. Each set of eight minor frames then includes 55 PROTEL science data words. There are 32 minor frames in each major frame, which is four sets of eight minor frames, or four sets of 55 science data words. Since PROTEL uses 55 science data words per spectrum, four complete sets of science data may be displayed in each major frame. These 55 science data words are the 55 entries in the science data format screen. Figure 12 notes the minor frame number location in the telemetry stream of the science data displayed. For example, in the HEA column, the data count corresponding to channel 10 will be from the third 11 bit science data word in minor frame numbers 1,9,17 or 25 of any given major frame.

## 2.5 Operation

PROTEL begins to accumulate data as soon as it is powered on. Under normal operation, it will continue to transmit data with no other commands needed until it is turned off. Periodically, however, the instrument will be put into a calibration mode and run through a testing sequence, to check for noise and to check detector gains. This sequence looks at the response of each individual detector to an internally generated ramp of standard pulses. The calibration sequence is begun by enabling the calibration pulser, (all 4 CALEN commands in the housekeeping display will go to 1) which sends a continuous ramp of pulses into the pulse height analyzers. Then all the detectors but one are made transparent, and the response of each single detector to the pulses is compared to data from previous calibration runs. Upon completion, all detectors are returned to normal operation, and the pulser is turned off. The housekeeping data will again show all zeroes. This calibration sequence is listed in detail in Table 6.

If the sequence shows that one of the detectors has become very noisy, or that its gain has changed considerably, it will be left transparent to the logic and no longer used. It is expected that LD1 will become radiation damaged within a year or two, but all the others should, barring unusual environments, last for the lifetime of the satellite.

MW# = MINOR FRAME WORD #



35

FO920 DISK1  
ACCUMULATED TELEMETRY DATA

25 AUG 86 08:37:33

Data for 9-AUG-86 10:49:17

Valid sets accumulated = 120

Beam Configuration: 0 DEG

92.0 MEV

3500 CTS/S

HEA			HED		LEA		LED		HI			
1	↓	294.	D1A	2	170544.	1	↓	D1A	↓	1	6	0.
2	0	279.	D12A	10	150832.	2	4	D12A	5	2	14	0.
3	8	62.	D123A	18	120376.	3	12	D13A	13	3	22	0.
4	16	113.	D134A	26	127376.	4	20	D134A	21	4	30	0.
5	24	431.	D145A	↓	120376.	5	28	D5	29	5	↓	0.
6		95.	D6	↓	100416.	6		D1	0.	6	7	0.
7	↓	363.	Dr	3	20402.	7	↓	D2		7	15	0.
8	↓	830.	D1	11	170576.	8	↓	D3		8	23	0.
9	1	285.	D2	19	252752.	→	0.	D4	↓	9	31	0.
10	9	2026.	D3	27	357632.			10	↓	0.		
11	17	579.	D4		316416.			→	0.			
12	25	8422.	D5	↓	378688.							
13		1867.										
14	↓	6603.										
15		4522.										
16	↓	24438.										
	→											

Figure 12. Science Data Word Telemetry Locations. The science data display with indications of which minor frame location is allocated to each word. For example, in the HEA column, the data count corresponding to channel 10 will be transmitted as the third 11-bit science data word in minor frame number 1, 9, 17, or 25 of any given major frame. For example, minor frame 3 of any given major frame contains, in the 10 S-35 blocks of Figure 10, the seven science data words (see Figure 11) for D6, Dr, D1, D2, D3, D4, and D5, in the HED column.

Table 6. Calibration Sequence

Test sequence of commands to be used periodically in orbit to check detector gains, noise, and DPU electronics. The sequence examines each detector individually and then checks each redundant logic circuit. One minute of data is read between each step.			
Step	Cells		Function
1.	all cells	0	Clear command system
2.	CALEN A	- 1	
	CALEN B	- 1	
	CALEN C	- 1	
	CALEN D	- 1	Enable calibration system
3.	HED2	- 1	
	HED3	- 1	
	HED4	- 1	
	HED5	- 1	
	HED6	- 1	Calibrate HED 1
	LED2	- 1	
	LED3	- 1	
	LED4	- 1	
	LED5	- 1	Calibrate LE D1
4.	HED1	- 1	
	HED2	- 0	Calibrate HE D2
	LED1	- 1	
	LED2	- 0	Calibrate LE D2
5.	HED2	- 1	
	HED3	- 0	Calibrate HE D3
	LED2	- 1	
	LED3	- 0	Calibrate LE D3
6.	HED3	- 1	
	HED4	- 0	Calibrate HED4
	LED3	- 1	
	LED4	- 0	Calibrate LED4
7.	HED4	- 1	
	HED5	- 0	Calibrate HED5
8.	HED5	- 1	
	HED1	- 0	Calibrate HED1
	LED4	- 1	
	LED1	- 0	Calibrate LED1
9.	HEMEM A, B, C, D	- 1	
	LEMEM A, B, C, D	- 1	Switch HE and LE memories to alternates
10.	COM2	- 1	Switch command system path to output
	COM3	- 1	shift register E, B path 2
11.	COM2	- 0	Switch command system path back
	COM3	- 0	to output shift register D, A path 1
12.	HESUM	- 1	
	LESUM	- 1	Switch off HE and LE summing
13.	all cells	- 0	Return instrument to operating mode

### **3. CALIBRATION AND TESTING**

#### **3.1 Brief Overview of Calibration Procedures**

The instrument was extensively calibrated and environmentally tested before delivery to the spacecraft manufacturers. The calibration procedures consisted of both radioactive source calibrations of the individual detectors to determine their charge-voltage relationships, and accelerator beam calibrations of the sensor heads and the DPU logic as a whole. The environmental tests included leakage current and temperature studies of the individual detectors and environmental testing of the entire instrument assembly, including shock and vibration, electromagnetic cleanliness, thermal vacuum testing, and thermal cycling.

The calibration and testing procedures will be described here in chronological order: individual detector testing done in the winter and spring of 1985 - 1986, environmental testing and calibrations done during the summer of 1986, satellite integration in 1986 - 1987, and refurbishment, retest, and recalibration in 1987 - 1988.

#### **3.2 Individual Detector Testing and Calibration**

##### **3.2.1 LOW ENERGY HEAD DETECTORS**

The first detectors to be tested were the Ortec surface barrier detectors for the Low Energy Head. Two detectors were obtained for each one needed, and leakage current measurements were used to screen for the best of each pair. The characteristics of the five chosen for use are listed in Table 2.

The ten Ortec detectors were tested under vacuum for periods of not less than four days each. All the detectors were stable and quiet. The ones chosen were those with the lowest average leakage current (at full bias, and at any temperature within the measured range), since the thickness differences between each pair are negligible, and the relative noise levels vary directly with the leakage current.

In the test setup, each detector was connected to a bias voltage supply and a preamplifier (see Figure 13). The detector was placed in a vacuum and the leakage current was monitored as a function of temperature, time, and bias voltage. The measured average leakage currents are listed in Table 7.

After determining that the detectors were stable and quiet, the next step was the determination of the relationship between charge deposited and voltage produced for each detector. Each detector was exposed to alpha particle radiation sources, including Americium, Californium, and Gadolinium. Table 8 lists the characteristics of these sources. To obtain a greater range of deposited energy values, some of the measurements were taken after first passing the alpha particles through different thicknesses of Mylar or aluminum.

Each of the five detectors was exposed to several different energies in this way, and the responses were recorded with a multichannel analyzer (MCA). The relationship of output pulse voltage (corresponding to an MCA channel number) to the calculated keV deposited in the detector was then fitted using a weighted linear regression. The buffer gains in the DPU were adjusted so that a 5.5 volt pulse corresponded to the maximum proton energy deposition in each detector. The MCA channel calibrations were then used as a standard in that given pulser inputs to the preamplifiers could be used

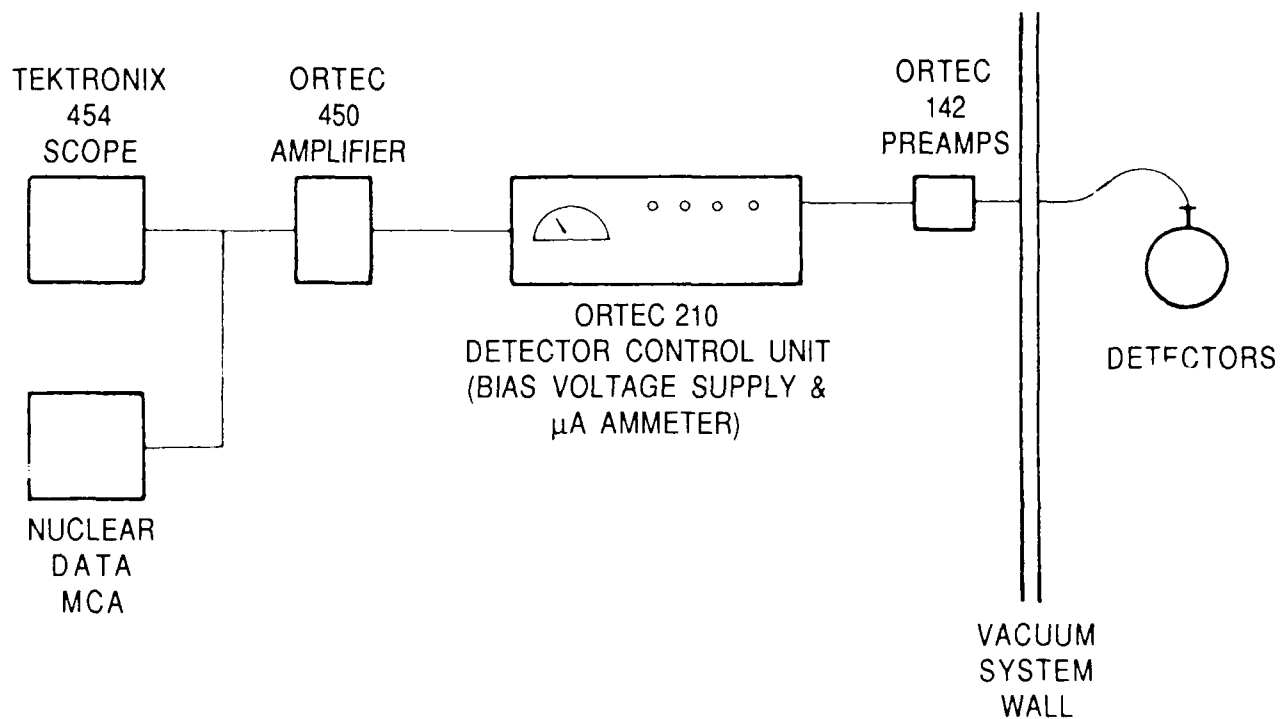


Figure 13. Preliminary Detector Test Setup



Table 7. Leakage Currents

Measured average leakage currents for each detector.						
	<u>Low Energy Head</u>					
	LD1	LD2	LD3	LD4	LD5	
Measured: (microamps)	.02 - .025	.21 - .22	.06 - .11	.22 - .32	.12 - .18	
Ortec Specifications: (microamps)	.07	.40	.15	.47	.36	
	<u>High Energy Head</u>					
	HD1	HD2	HD3	HD4	HD5	HD6
Measured: (microamps)						
Active Region	.05	1.24	2.7	.41	1.5	4.5
Ring Area	.63	3.4	1.5	5.2	5.8	-
Manufacturer Specifications: (microamps)						
Active Region	*	1.78	1.58	1.65	1.96	8.0
Ring area	*	5.62	4.72	8.55	10.74	-

\*: HD1 total = .88

Table 8. Alpha Source Characteristics

Gadolinium 148	AF-148,	F-251, Capsule A-2 9/15/83, PO# A1614 9.21 $\mu\text{gm}/\text{cm}^2$ 100 - 200 $\mu\text{gm}/\text{cm}^2$ Au cover +/- 15%
Americium 241	AF-241,	F-251, Capsule A-2 6/15/83, PO# A1641 352 $\mu\text{gm}/\text{cm}^2$ 100 - 200 $\mu\text{gm}/\text{cm}^2$ Au cover +/- 15%
Californium 252	FF-252,	Dec., 1979, PO# 3074
The sources were made by:		Isotope Products Laboratories 1800 N. Keystone St. Burbank, CA 91504 (818) 843-7000

to simulate alpha particle depositions in the detectors. Figure 14 shows the alpha source calibration setup and the pulser simulation setup.

Using the relationship between energy deposited in each detector and the channel of the resulting peak on the MCA, the logical discriminator levels in the DPU were set. These discriminators determine, for each detector, if the amount of charge deposited in the detector by a particle is above or below a certain value by analyzing the output pulse height. This is the basis for the more complicated logic system which determines in which incident energy channel a valid event belongs. The deposited energy values measured by the discriminators are compared with deposited energies in the other detectors and evaluated to determine if they form a valid event.

An example of the process for setting the discriminator thresholds is as follows. The threshold for each detector is set separately. Table 1 shows that for detector 1, the discriminator threshold between channels 2 and 3 is a deposition of 0.945 MeV. The charge deposition in the detector corresponding to the desired incident energy can be simulated with a pulser input to the HD1 preamplifier. This pulser input to detector 1's preamplifier is thus adjusted so that it simulates a 0.945 MeV deposition. Because of noise in the system, the pulse will have an approximately gaussian distribution about the central voltage.

Next we command the logic system into a "D1 cal" setup, a mode in which all logic decisions are made by detector 1. Thus if detector 1 receives a deposition between the deposition limits for a given channel, a count will register in that channel in the science data display, independent of any other detector. With the pulser centered about 0.945 MeV (simulated), we adjust the discriminator level (by varying a resistor in the DPU) until we see as many counts in channel 2 as we see in channel 3. This means that the discriminator setting has been set to 0.945 MeV. The process is then repeated for each level and for each detector. In the Low Energy Head, most levels were set to within 10 keV of the desired settings. (See Table 16.)

Once all of the levels were set, the variable resistors were replaced with fixed value resistors.

### 3.2.2 HIGH ENERGY HEAD DETECTORS

Detector testing procedures for the High Energy Head were basically the same as for the Low Energy Head, but with the added complexity of the guard ring systems. Each of the High Energy Head detectors, except for the sixth, is a two-detector system constructed from one piece of silicon. The center region of the detector is the active counting region, and the annular ring about the edge is the active shielding, or veto region. (See Figure 3.) Events in a detector which are coincident with events in a ring are rejected as false. Since leakage current is an edge effect in these detectors, the guard ring also serves the purpose of significantly reducing the central area leakage current, and resulting noise, by containing most of the detector's leakage current in the ring area.

The first test of these detectors was the measurement of their leakage current and stability. The test setup was the same as for the Low Energy Head testing, shown in Figure 13, except that there were two bias voltage connections and two preamplifiers for each detector, one for the center and one for the ring. The measured leakage currents are listed in Table 7.

The next test was a thermal cycling of the SiLi detectors to ensure that their sonic bond connections were secure. The High Energy Head detectors (except for HD1) do not use surface contacts as do the Low Energy Head detectors. Instead, signal and bias connections are made with sonically

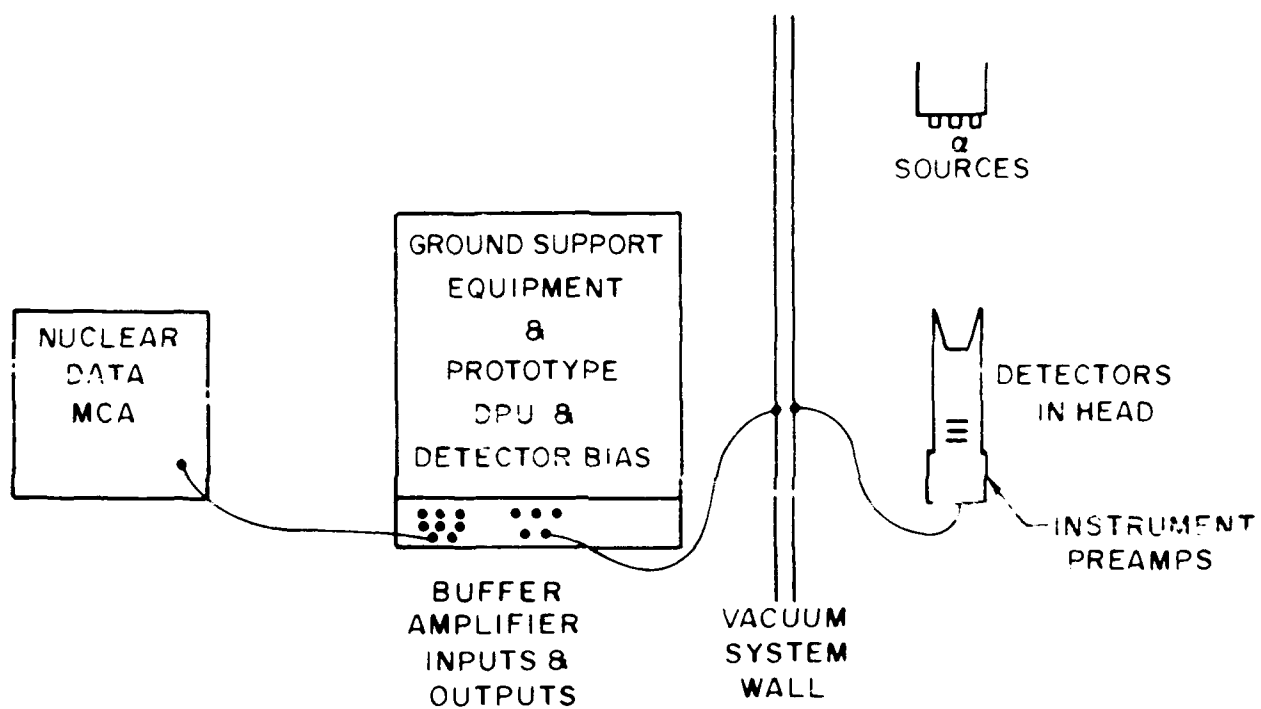


Figure 14. Alpha Source Test Setup

bonded 0.7 mil Al wire. The detectors were connected to a bias supply and cycled in vacuum from -10°C to room temperature. There were no visible permanent effects.

The next step was the determination of the charge deposited vs. voltage produced for each detector and for each ring. Because the lithium dead layer on the silicon-lithium drifted detectors, HD2 - HD6, severely degraded the alpha peak, it was necessary to expose the rear side of each detector to the alpha particles, not the front side. This is only a problem when calibrating with heavy particles such as alphas, because of their relatively short ranges, although the negligible effect on protons was taken into account in the design. Otherwise, the procedure and setup were as described for the Low Energy Head, with the addition of repeating the process for each ring. The buffer gains were adjusted so that the maximum of the proton energy deposition curve in each detector corresponded to a voltage of approximately 5.5V.

One further environmental test was done on the SiLi detectors. The sonic bond electrical connections on the detectors were pull tested to non-destructive levels, less than 1.2 g, at Assurance Technology Corporation in Chelmsford, MA. Each bond wire was pulled upwards at its center with a force of between 1.1 and 1.2 g, and was visually inspected. All of the bonds withstood the test, with no visible lifting from the bonding pads.

The discriminator levels were set in the same manner as was described for the Low Energy Head. The levels were set in accordance with Table 1. Most of the levels were set to within 25 keV of the desired settings. (See Table 16 in Section 3.7.) The threshold levels for the ring detectors were set just above their low level noise threshold, at 2.5 MeV. Note that although there are five ring detectors, there are only two ring threshold levels to set, since the ring outputs for HD1 and HD2 are tied to one preamplifier, and the ring outputs for HD3, HD4, and HD5 are tied together to another preamplifier. The level for the anticoincidence detector, HD6, was set to 2.5 MeV.

### **3.3 Environmental Testing**

The instrument was subjected to a series of environmental tests, including shock and vibration, electromagnetic cleanliness, thermal cycling, and thermal vacuum cycling. The tests were done in accordance with the requirements of the Interface Control Document (ICD)<sup>16</sup> for the CRRES satellite. The test data and results are listed in detail in the ICD Compliance Documentation for AFGL-701-8/9.<sup>17</sup>

The specifications for the shock and random vibration test are listed in Table 9. The three parts of the instrument were shaken and shocked separately on the Unholtz-Dicke 1000 shaker at Draper Laboratories in Cambridge, MA. There was no visible damage to flight parts. One of the DPU printed circuit boards became unseated during shake. It was resealed and all of the boards were then spot bonded with epoxy. A second shake test of the DPU showed that the boards were then secure.

---

16. CRRES ICD (7 March 1989) Revision G, Ball Space Systems Division, Boulder CO.

17. Compliance Data Package for PROTEL, Ball Space Systems Division, Boulder, CO.

Table 9. Shock and Vibration Test Specifications

The test items were subjected to environmental testing in accordance with test specification CRRES-226, Rev. D. The vibration is per Paragraph 4.3.1 and the shock per Paragraph 4.3.5, Figure 8.	
Vibration:	Initial Slope: +6dB/OCT from: 16 Hz to 48 Hz Intensity: 0.10 g <sup>2</sup> /Hz from 48 Hz to 400 Hz Final Slope: -6dB/OCT from 400 Hz to 2048 Hz Composite Spectrum: 8.292 GRMS Duration: One minute each axis
Shock:	Shape: Half sine Level: 40 g, +/- 6g Duration: 11 milliseconds Two shocks each axis, Positive and Negative

The electromagnetic compatibility test was done at Sanders Associates in Nashua, New Hampshire. The test was run according to the military standard 461B.<sup>18</sup> The first conducted emissions test showed that the DPU needed a reconfiguration of the wiring harness. The harness was rebundled and a filter was inserted at the spacecraft interface. A retest showed a major improvement. A complete set of test data is available in Reference 17.

Thermal vacuum cycling was done in the MUMBO chamber at AFGL. The three pieces were placed on the thermal platen as shown in Figure 15, with indium sheets placed between the pieces and the platen for better heat conduction. A heavy aluminum shroud was placed over the two sensor heads to form a radiative oven. The shroud and the DPU were then covered with an aluminized Mylar sheet to reflect away the chamber wall temperature. The simulated spacecraft line passed through a connector port to the GSE console located alongside the chamber. The platen temperature was automatically controlled with thermocouples. Thermistors were mounted to various spots on the instrument and shroud, and were monitored along with the thermistors built into the PROTEL electronics.

The flight instrument was subjected to three thermal/vacuum cycles as shown in Figure 16. The temperature was controlled 24 hours a day. The chosen test limits were -20°C and +30°C, 5 - 10°C beyond the ICD operating limits of PROTEL. At each temperature extreme, the functional test outlined in Table 6 was run, to test all the commands and noise levels.

---

18. Military Standard 461B.

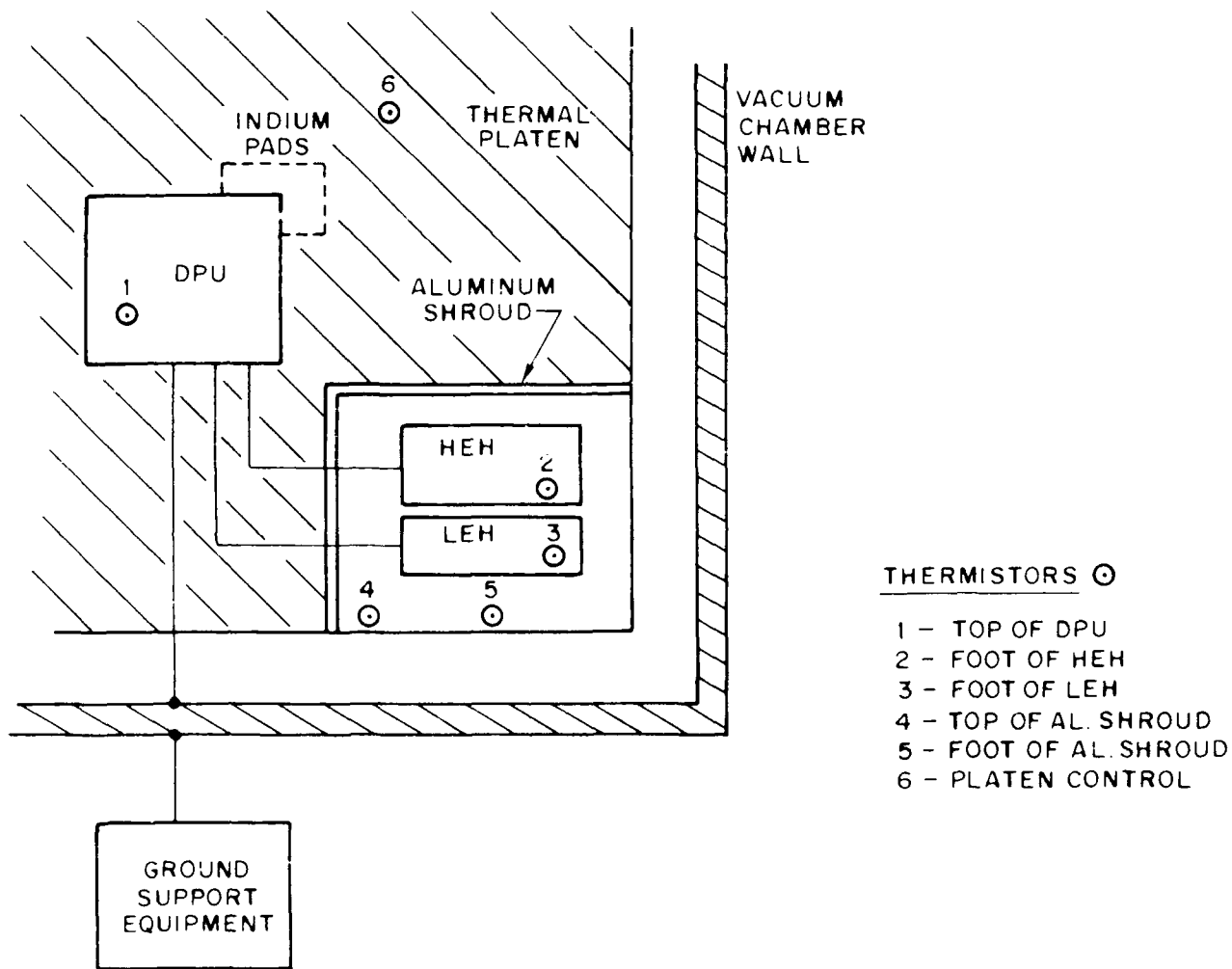


Figure 15. Thermal Vacuum Test Setup

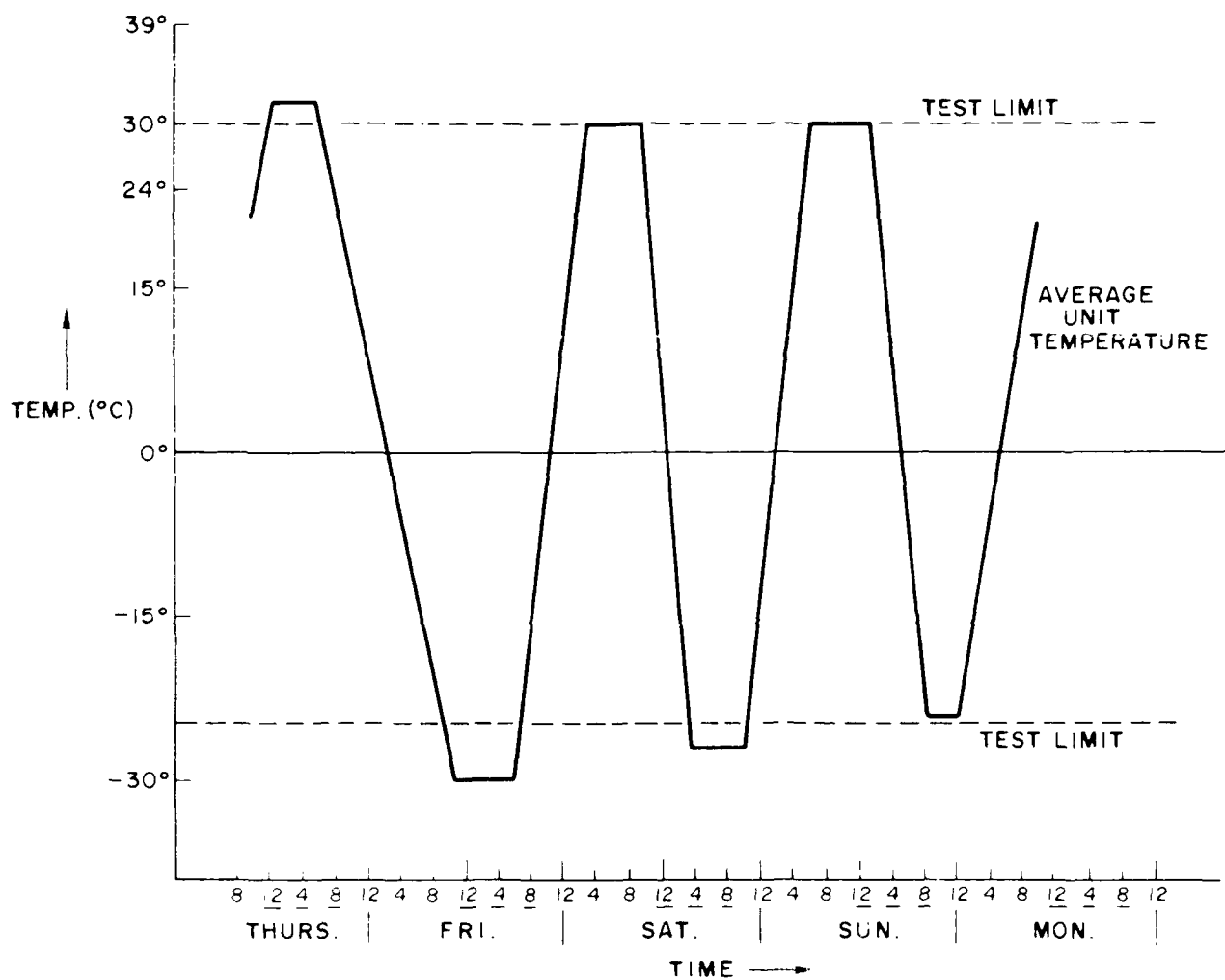


Figure 16. Thermal Vacuum Test Cycles

Data was recorded during a pre-vacuum test, a room temperature vacuum test, and in vacuum at each cycle extreme. An anomaly was noted in the data at low temperatures which was traced to a resistor in the DPU of marginally incorrect value. This resistor was replaced, and the anomaly was not seen again.

The thermal cycle (not under vacuum) test was done at the MIT Center for Space Research in a small laboratory thermal chamber. The three pieces were sealed in plastic bags which were filled with dry nitrogen, and the chamber itself was filled with carbon dioxide. The simulated spacecraft line passed through a hole in the side of the chamber to the Ground Support Equipment (GSE) alongside. A thermistor was attached to the surface of the High Energy Head, and was monitored along with the thermocouples built into the PROTEL electronics.

The instrument was subjected to four thermal cycles as shown in Figure 17. The temperature was monitored constantly. The chosen test temperature limits were  $-25^{\circ}\text{C}$  and  $+30^{\circ}\text{C}$ ,  $5^{\circ}$  -  $10^{\circ}\text{C}$  beyond the ICD operating limits of PROTEL. The instrument was placed in standby mode (off except for a small bias applied to the detectors) during temperature changes, and was left in standby mode for at least one hour before each hot or cold start. At each temperature extreme, the functional test in Table 6 was run, to check all commands and noise levels.

The instrument responded normally within its operating temperature limits. Beyond the low temperature operating limit, some noise appeared in the Low Energy Head detectors, but no damage was sustained and the noise disappeared when the temperature was raised.

For both the thermal vacuum and thermal cycle tests, all data recorded are listed in Reference 17. Further environmental testing was done after the instrument was returned from the spacecraft manufacturer for pre-flight storage. (See Section 3.6.)

### **3.4 Accelerator Beam Calibrations - Procedures and Setup**

In order to determine the integrity and efficiency of the instrument as a whole, to verify the individual detector calibrations, and to check the discriminator settings, the instrument was calibrated at three proton accelerator beam facilities of energies ranging from 1.5 MeV to 100 MeV. In addition, the Low Energy Head was calibrated for ions.

The accelerators were at three different sites. The first calibration, with the University of Pittsburgh Nuclear Physics Laboratory tandem van de Graaff accelerator, encompassed measurements over the largest range of energy. They included calibrations of the Low Energy Head for protons from 1.5 to 9 MeV, and for ions from 21 to 60 MeV, and of the High Energy Head for protons from 6 to 19.5 MeV. The second calibration, at the Princeton University John Henry Laboratory cyclotron, covered the middle energy proton range of the the High Energy Head, from 25 to 40 MeV. The third calibration, at the Harvard University cyclotron, covered the highest energy protons, from 33 to 100 MeV.

Tables 10, 11, and 12 list the calibration measurements made at the Pittsburgh, Princeton, and Harvard facilities, respectively. The different types of proton measurements listed are as follows. A "full", or "F" measurement is taken with the instrument in its normal operating mode. A "Dx" Table measurement is a detector calibration, where all logic decisions are made by detector Dx alone. A



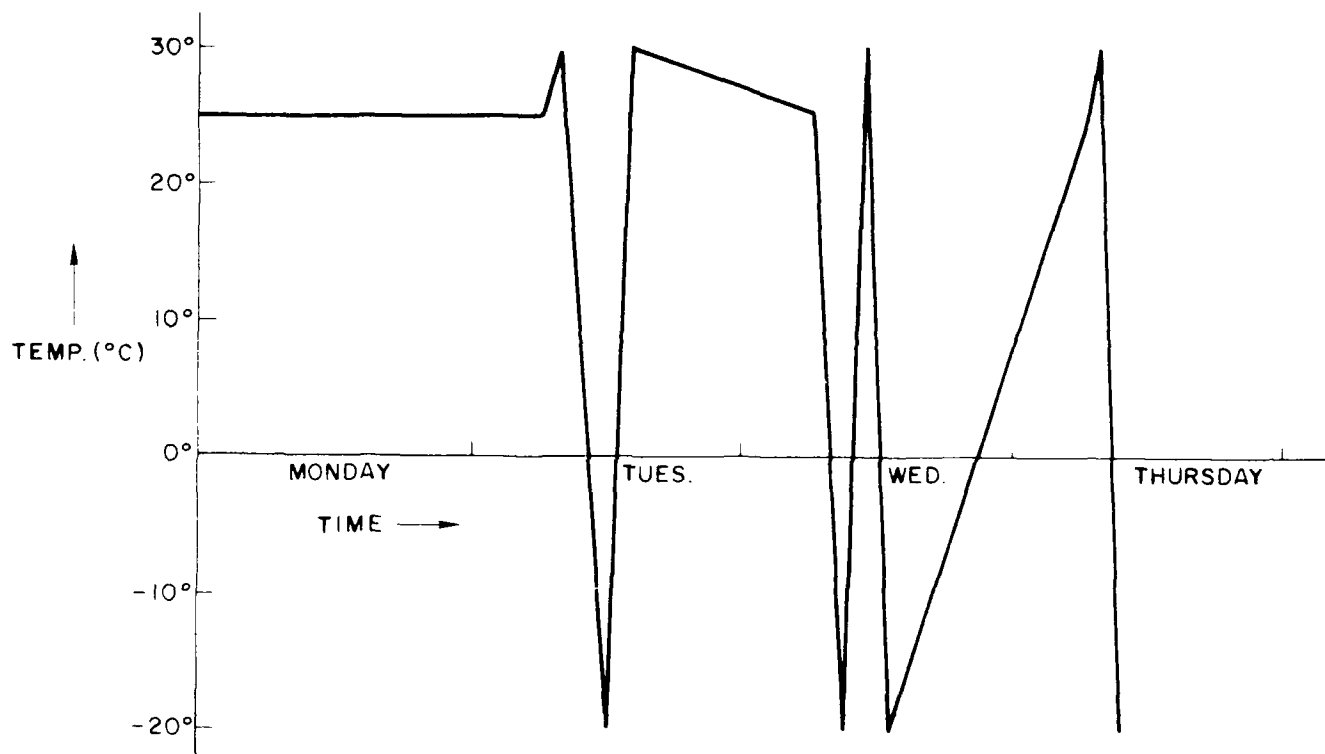


Figure 17. Thermal Test Cycles

Table 10. Pittsburgh Van de Graaf Accelerator Runs

The types of runs listed are as follows: (F) full logic; (N6NR) full logic with detector 6 and the rings transparent; (D#) system in calibrated mode with only detector (#) operating.

<u>1986</u>		
Energy (MeV)	Type	Comments
High Energy Head:		
5.889	F	
5.990	F	
6.090	F	Lower measured boundary of channel 1
6.190	F	
6.390	F	
6.590	F	
6.790	F	
6.991	F	
7.190	F	
7.391	F	
7.491	F	
7.565	F	Measured channel 1/2 boundary
7.641	F	
7.791	F	
7.992	F	
8.192	F	
8.392	F	
8.592	F	
8.792	F	
8.992	F	
9.192	F	
9.342	F, D1	
9.442	F, D2	Measured 2/3 boundary
9.542	F	
9.692	F, D1, D2	
9.892	F	
9.932	D1	D1's measured 3/4 boundary
10.043	F	
10.053	F	Measured 3/4 boundary
10.131	D2	D2's measured 3/4 boundary
10.113	F	Nominal 3/4 boundary
10.243	F	
10.393	F	
10.593	F, D1, D2	
10.993	F, D1, D2	
11.093	F, D1	
11.193	F, D1, D2	D1's measured 4/5 boundary
11.293	F, D1	

Table 10. Pittsburgh Van de Graaf Accelerator Runs (Cont.)

<u>1986 (Cont.)</u>		
Energy (MeV)	Type	Comments
11.353	F, D2	
11.400	F	
11.413	F	Measured 4/5 boundary
11.443	F	
11.493	F, D2	D2's measured 4/5 boundary
11.517	D2	
11.593	F, D1, D2	
11.793	F, D1, D2	
12.094	F, D1	
12.394	F, D1	
12.694	F, D1, D2	
12.994	F	
13.294	F, D1, D2	
13.594	F, D1	
13.894	F, D1, D2	
14.194	F, D1, D2	
14.494	F, D1, D2	
14.524	D1	D1's measured 5/6 boundary
14.794	F, D1, D2	
14.854	F, D3	Measured 5/6 boundary
10.793	F, D1, D2, D3, D4, D5	15 degrees off angle
Low Energy Head:		
1.757	F	
1.878	F	
1.938	F, D1, D2	
2.043	D1, D2	D2 1/2 boundary
2.068	D1	D1 2/3 boundary
2.078	FN1	
2.129	FN1, D1, D2	
2.181	FN1	
2.213	FN1	
2.276	D2	D2 2/3 boundary
2.331	FN1	
2.397	D1	D1 3/4 boundary
2.531	D1, D2	
2.595	D1	D1 4/5 boundary
2.616	F, D1	
2.631	D2	
2.731	FN1	
2.812	D3	D3 3/4 boundary
2.832	FN1	

Table 10. Pittsburgh Van de Graaf Accelerator Runs (Cont'd)

1986 (Cont'd)		
Energy (MeV)	Type	Comments
2.903	FN1, D1, D3	
2.983	FN1	
3.083	F, D1, D2, D3	
3.091	F, FN1	
3.156	FN1	
3.158	D3	D3 4/5 boundary
3.184	FN1, D3	
3.284	FN1, D2, D3	
3.384	FN1	
3.484	F, D1, D2, D3, D4	
3.585	FN1, D1, D2, D3, D4	
3.684	F, D1, D2, D3	
3.785	F	
3.835	FN1	
3.885	F, D1, D2, D3, D4	
3.925	F, D1, D3	5/6 boundary
3.955	D2	D2 5/6 boundary
3.985	F, D1, D2, D3, D4	
4.035	F	
4.185	F, D1, D2, D3, D4	
4.386	F	
4.587	F, D2, D3, D4	
4.669	FN1, D4	D4 6/7 boundary
4.729	FN1	
4.786	FN1, D3	D3 6/7 boundary
4.988	FN1	
5.388	FN1, D3, D4	
5.989	FN1	
6.490	FN1	
7.091	FN1	
7.201	FN1	
7.291	FN1	
7.541	D3	D3 7/8 boundary
7.791	FN1	
8.292	FN1, D1, D3, D4	
8.492	D1	D1 channel 8 upper edge
8.792	FN1, D4	
8.892	FN1	
8.992	FN1, D1	
9.393	D3	D3 channel 8 upper edge
9.492	FN1	D5 threshold
10.393	F	
2.883	F, FN1	High count rate (30K/sec)
4.195	F, FN1	High count rate (30K/sec)

Table 10. Pittsburgh Van de Graaf Accelerator Runs (Cont'd)

<u>1986</u> (Cont'd)		
Energy (MeV)	Type	Comments
Low Energy Head Ions:		
32.5	Carbon	
38.0	Carbon	
41.0	Carbon	
42.9	Carbon	
47.8	Oxygen	
54.2	Oxygen	
<u>1987</u>		
Low Energy Head:		
1.370	F	
1.758	F, D1	
1.773	F, D1	
1.874	F, D1	
1.915	F, D1	
1.925	F, D1, D2	
1.935	F, D1, D2	
1.945	F, D1, D2	
1.955	F, D1, D2	
1.965	F, D1, D2	
1.975	F, D1, D2	
1.985	F, D1, D2	
1.995	F, D1, D2	
2.005	F, D1, D2	
2.015	F, D1, D2	
2.025	F, D1, D2	
2.045	F, D1, D2	
2.065	F, D1, D2	
2.105	F, D1, D2	
2.145	F, D1, D2	
2.176	F, D1	
2.185	F, D1, D2	
2.225	F, D1, D2	
2.235	F, D1, D2	
2.245	F, D1, D2	
2.270	F, D2	
2.295	F, D1, D2	
2.345	F, D1, D2	
2.397	F, D1, D2	
2.447	F, D1, D2	
2.497	F, D1, D2	

Table 10. Pittsburgh Van de Graaf Accelerator Runs (Cont'd)

<u>1987</u> (Cont'd)		
Energy (MeV)	Type	Comments
2.547	F, D1, D2	
2.597	F, D1, D2	
2.606	F, D1	
2.647	F, D1, D2, D3	
2.697	F, D1, D2, D3	
2.760	F, D1, D2, D3	
2.792	F, D1, D2, D3	
2.800	F, D1, D2, D3	
2.813	F, D3	
2.840	F, D1, D2, D3	
2.880	F, D1, D2, D3	
2.920	F, D1, D2, D3	
2.960	F, D1, D2, D3	
3.000	F, D1, D2, D3	
3.040	F, D1, D2, D3	
3.149	F, D3	
3.228	F, D2	
Additional Energies:		
3.228, 3.284, 3.384, 3.484, 3.584, 3.684, 3.784, 3.884, 3.934, 4.004, 4.035, 4.135, 4.235, 4.335, 4.435, 4.535, 4.635, 4.715, 4.735, 4.765, 4.785, 4.985, 5.236, 5.486, 5.737, 5.987, 6.237, 6.239, 6.488, 6.489, 6.738, 6.739, 6.988, 6.989, 7.239, 7.489, 7.639, 7.739, 7.740, 7.989, 8.24, 8.49, 8.74, 8.99, 9.24, 9.49, 9.991		

Table 10. Pittsburgh Van de Graaf Accelerator Runs (Cont'd)

1987 (Cont'd)		
Energy (MeV)	Type	Comments
Low Energy Head Ions:		
19.1	Carbon	
25.0	Carbon	
21.0	Carbon	
22.5	Carbon	
22.75	Carbon	
27.0	Carbon	
30.0	Carbon	
29.0	Carbon	
32.7	Carbon	
35.0	Carbon	
38.85	Oxygen	
45.0	Oxygen	
50.0	Oxygen	
55.0	Oxygen	
52.8	Oxygen	
53.0	Oxygen	
60.0	Oxygen	
High Energy Head:		
5.99, 6.08, 6.24, 6.49, 6.74, 7.00, 7.24, 7.49, 7.57, 7.64, 7.74, 8.00, 8.24, 8.49, 8.74, 8.99, 9.24, 9.43, 9.44, 9.75, 9.92, 10.0, 10.04, 10.12, 10.24, 10.49, 10.74, 10.99, 11.18, 11.24, 11.40, 11.51, 11.74, 11.99, 12.32, 12.56, 12.99, 13.32, 13.56, 13.99, 14.32, 14.41, 14.84, 14.90, 14.19, 11.24, 9.44, 10.66		

Table 11. Princeton Accelerator Runs

The types of runs listed are as follows: (F) full logic; (D#) system in calibrated mode with only detector (#) operational; (N) a run taken with only neutrons in the beam.		
1986		
Energy (MeV)	Type	Comments
High Energy Head:		
40.12	N	Initial beam energy = 40.19
40.12	F	
38.72	F	
37.98	F, D4, D5, N	Improper 10/11 split
37.65	F, D4, D5	
37.56	F, D4, D5	
36.00	F, D4, D5, D3, N	
35.42	F, D3, D4, D5, N	
34.61	D3, D4, D5, N	New beam energy - 30.12
30.08	F, D1, D2, D3, D4, D5, N, N(D2), N(D4), N(D5)	
27.25	F, D4, D5	
27.01	D1, D3, D4	Low efficiency
25.97	F, D1, D2, D3, D4, N	
25.13	F, D1, D2, D3, D4, N	
24.68	F, D1, D2, D3	



Table 12. Harvard Cyclotron Runs

The types of runs listed are as follows: (F) full logic; (N6NR) full logic with detector 6 and the rings transparent; (D#) system in calibrated mode with only detector "#" operational.		
<u>1986</u>		
Energy (MeV)	Type	Comments
High Energy Head:		
100.0	F	FWHM = 4 MeV
92.0	F, D1, D4, D5	
83.4	F, D1, D4, D5	
73.1	F, D1, D4, D5	
70.1	F, D1, D4, D5	
66.6	F, D1, D4, D5	
64.9	F, D1, D4, D5	
62.2	F, D1, D4, D5	
59.0	F, D1, D4, D5	
56.2	F, D1, D4, D5	
54.6	F, D1, D4, D5	
53.5	F, D1, D4, D5	
52.9	F, D1, D4, D5	
50.1	F, D1, D4, D5	
48.0	F, D1, D4, D5	
43.9	F, D1, D4, D5	
41.0	F, D1, D4, D5	
38.6	F, D1, D4, D5	Beginning of overlap w/Princeton
37.9	F, D1, D4, D5	
34.8	F, D1, D3, D4, D5	
<u>1988</u>		
34.8	F, N6NR, D2, D3, D4, D5	
37.9	F, N6NR, D2, D3, D4, D5	
43.9	F, N6NR, D4, D5	
50.1	F, N6NR, D3, D4, D5	
53.5	F, N6NR, D3, D4, D5	
56.2	F, N6NR, D4, D5	
59.0	F, N6NR, D4, D5	
62.2	F, N6NR, D5	
66.6	F, N6NR, D4, D5	
70.1	F, N6NR, D4, D5	
73.0	F, N6NR, D4, D5	
87.6	F, N6NR, D4	
100.	F, N6NR, D4, D5	
34.8	Low Energy Heads	
34.8 with degrader L72	Low and High Energy Heads	
34.8 with degrader L72 and L77	Low and High Energy Heads	
70.1 and 87.6	HEH at different distances from end of beam	
70.1	HEH at 10 degree incident angle	
100.	HEH and LEH, incident to side of heads	

"boundary", or "B" measurement is taken at the energy that registered the same number of counts in two adjacent channels, with the system in either a normal or calibrated mode.

"boundary", or "B" measurement is taken at the energy that registered the same number of counts in two adjacent channels, with the system in either a normal or calibrated mode.

For the ion measurements, since they concern only LD1, there were no detector calibration measurements. The "I" measurements are calibrations of the ion logic system with ions of the stated energy and mass. The "IB" measurements are calibrations of the nominal ion channel boundaries. Ion measurements were taken at the Pittsburgh van de Graaff only.

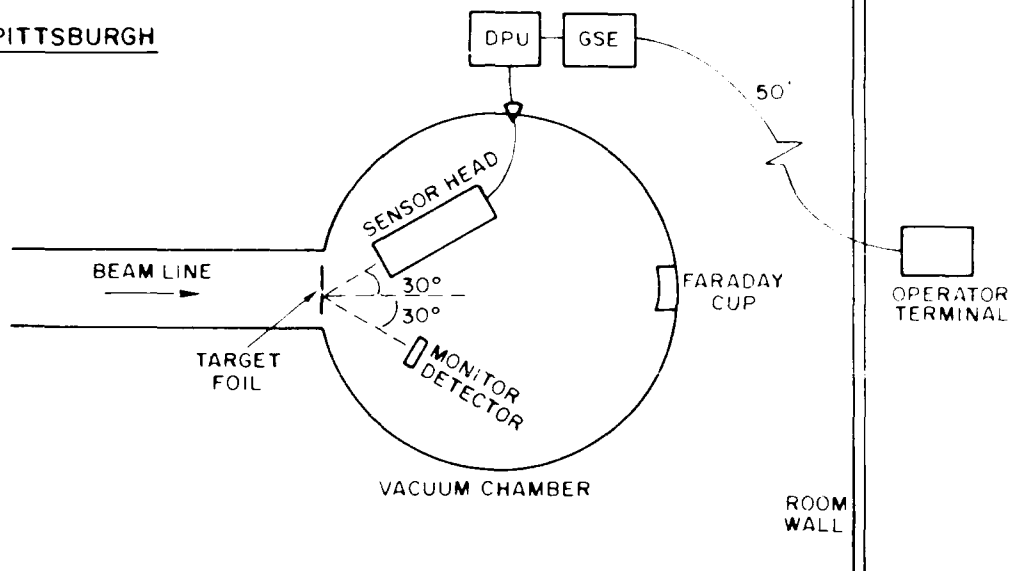
The boundary measurements are one of the two main reasons for the accelerator calibrations. The boundaries are measured in two ways: by use of the full logic system, or by use of the individual detectors with the system in the calibrated mode. Differences between detectors in determining a particular boundary produce energy ranges between channels in which particles are not measured, and this affects the overall response function. This response function is the second important goal of the calibrations.

As an example, consider the boundary between High Energy Head channels number 5 and 6. Nominally, this boundary was set during the discriminator level setting process (see Section 3.2) at an incident energy of 14.92 MeV. However, the accelerator calibration shows this level to be at 14.854 MeV. That is, with the proton beam tuned to 14.854 MeV, the energy spread in the beam produces an equal number of counts in channels 5 and 6. Now, if we look at the determination of this level by each detector individually, by making detector calibration measurements at different energies, we find that if the decision between channel 5 and 6 is made solely by detector 1, the incident boundary energy is 14.524 MeV. However, if the decision is made by detector 3, (a D3 calibration) the boundary is 14.914 MeV.

The combination of D1 being a little low and D3 a little high creates an energy range in which the protons are not measured. This is because any particle with an energy between 14.524 MeV (D1's determination) and 14.914 MeV (D3's determination) will be registered in channel 6 by detector 1, but in channel 5 by detector 3. Since the voting must be unanimous, the particle is rejected as a false count, and the proton is not counted in either channel. There is a similar situation at each boundary, between every channel, in both heads. This has a significant effect on the response function, but there are other effects, such as detector noise and particle straggling, which also affect the overall instrument efficiency. The measurement of the response curves which incorporate these effects is the final goal of the calibration measurements.

The setup was basically the same for each of the three calibrations. The sensor head to be calibrated was placed inside a vacuum chamber attached to the end of the beam line (except at Harvard, where no vacuum chamber was necessary). The DPU was set outside the chamber and connected to the sensor through the vacuum wall. At Pittsburgh and Princeton, the incident beam was scattered through a target foil before reaching the sensor head, to cut down the beam intensity. At Harvard, the beam was degraded through lucite blocks. The support equipment was put outside the target room and connected by a long cable to the DPU. See Figure 18 for typical setups. The results of these and further (post-integration) calibrations are described in Section 3.7.

PITTSBURGH



HARVARD

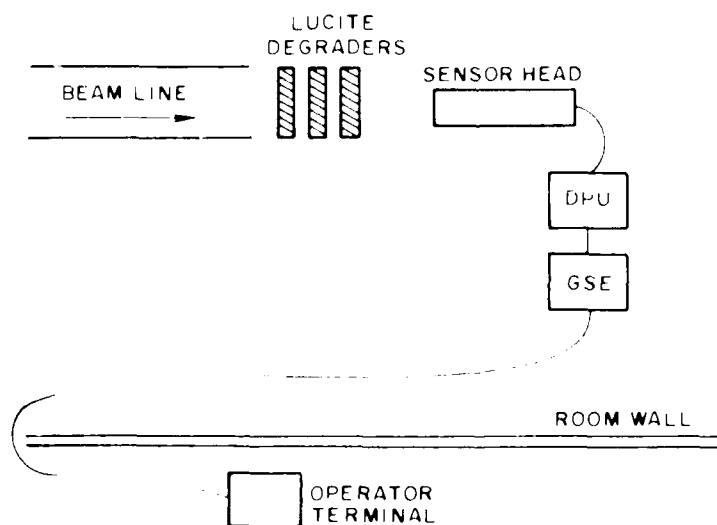


Figure 18. Accelerator Calibration Setup

### **3.5 Satellite Integration**

PROTEL was integrated onto the CRRES satellite at Ball Aerospace Systems Division, in Boulder, Colorado, in the fall of 1986. The satellite as a whole underwent environmental and other integration testing through the winter and spring of 1987. When the testing was completed, the instruments were removed from the satellite because of delays in the launch schedule. PROTEL was returned to AFGL in the summer of 1987, for storage and refurbishment.

During the course of the integration testing, three problems developed which would be attended to during the pre-flight storage period. First, it was determined that compensation magnets were needed on the HEH, to counteract the field of the electron-sweeping magnet. Second, during the thermal vacuum cycling of the full satellite, there was a failure of the high voltage converters in the DPU which supply the detector biases. And third, a detailed examination of the calibration data made it clear that several adjustments needed to be made to the discriminator level settings, and a change made to the logic, in the LEH.

### **3.6 Refurbishment and Recalibration**

The first refurbishment to be done was the replacement of the damaged voltage converters. The parts that failed were miniaturized Technetics 225 volt and 300 volt converters. They were both removed, and replaced with a single, non-miniature, 500 volt Technetics 3-watt converter. Because of the larger size of the new converter, it was mounted on the inside wall of the DPU, rather than on the converter board. The DPU was run in a vacuum with the new converter being monitored for temperature, and no problems were seen.

Next, some changes were made to the DPU logic and discriminator level settings, based upon a review of the first accelerator calibrations. Following this, a full recalibration of the LEH, and a partial one of the HEH, was done at the Pittsburgh accelerator, in November of 1987. The results of this calibration are discussed in the next section.

Because of the electronic and structural changes that had been made to the DPU, it was necessary to repeat some of the environmental tests. The EMC test at Sanders was repeated in January of 1988, and the DPU was vibration tested at the AFGL facility in February. The DPU shake showed no problem with the new converter mount, but the problem with the printed circuit boards shaking loose reappeared. This problem was fixed by putting a positive stop to the boards' motion in the form of viton rubber and Delrin plastic strips across the inside of the top of the DPU. When the top is bolted down, it exerts a positive pressure on the boards in three places on each board. The shake test was repeated, and no problems were seen.

Another shake test was done at the same time. The flight unit HEH detectors in their new mounts (involving notches and pins in HD4, HD5, and HD6 to avoid rotation of the detectors in their mounts) were not shaken in the original HEH vibration test. This test was done in January of 1988, and no problems occurred.

Following these shake tests, the entire instrument was put into the thermal vacuum facility at AFGL, and was cycled three times from  $-15^{\circ}\text{C}$  to  $+35^{\circ}\text{C}$ . No problems were noted.

The compensation magnets supplied by Ball Aerospace were bonded onto the HEH preamplifier cover using a NASA approved RTV epoxy and primer. The covers, with the magnets attached, were put

onto the prototype HEH assembly, and the unit was shake tested at the AFGL facility in June of 1988. The magnets were securely fastened.

Another developmental test was done at this time, using the AF/RADC linear electron accelerator to measure the effectiveness of the electron sweeping magnets. The instrument was set in front of a very low current 8 MeV electron beam. A 750 micron surface barrier monitor detector with a 0.5 inch diameter active area was positioned next to the head assemblies. When the monitor detector was receiving at least 20 counts per second, the sensor heads were seeing less than 4 counts per second in the HEH thickest detectors, and about .01 counts per second in the LEH thickest detector. This was with the beam directed straight into the head assemblies. With the beam hitting the side of the heads, the HEH saw less than 0.5 counts per second, and the LEH less than 0.05 counts per second. All of these counts were in the raw data only. All of the data for the above environmental and developmental testing are available in volume 3 of Reference 17.

Finally, because of the long wait between the instrument development and the satellite launch, it was decided that the High Energy Head detectors would need to be replaced before launch, because of the sensitivity of the SiLi type detectors. Hence, after all the rework was finished, the instrument was brought back to the Harvard cyclotron for a recalibration. This recalibration will be used as a standard by which to check the similarity of the new detectors to the ones which they will replace.

### 3.7 Calibration Results

There were two goals for the calibrations described above. The first was the measurement of the discriminator settings which form the channel boundaries. The second was the determination of the response function across the energy range of the instrument. The measured channel boundaries for the High Energy Head, the Low Energy Head, and the heavy ions are shown in Tables 13, 14, and 15. The response curves are shown in Figures 19 and 20.

Most of the discriminators were set within 10% of the desired settings. Table 16 shows, for each discriminator, the ratio of the measured level to the original design level. As was described in the previous section, differing channel borders among the detectors result in energy ranges over which protons are not measured. These energy ranges encompass 14.5% of the HEH spectrum, and 9.85% of the LEH spectrum. The heavy ion spectrum is unaffected, since only one detector is involved. The energy dependent response function of the instrument was defined to be, for a given incident energy beam measurement, the ratio of events in the appropriate channel to events in the raw, single detector data. This is an internal efficiency, and assumes that the raw data represent 100% of the environment. This ratio incorporates efficiency losses from timing problems between the detectors, from anomalous energy losses and straggling in the detectors, and from energy ranges between channels where no protons are measured. Figures 19 and 20 show the responses for the High and Low Energy heads. The predominant cause of loss of efficiency is the energy ranges between channels. Second are losses from anomalous energy depositions. (The efficiencies of the higher energy channels are lower in both heads because more detectors, and thus more straggling, are involved.) Thirdly, the LEH has losses from timing/count rate restrictions in the higher end of its range. Table 17 lists the average internal efficiency of each channel. Note that all responses listed here are for a flat spectrum, unidirectional incident beam.

Table 13a. Empirical Channel Boundaries - HEH-Pittsburgh Data

Channel borders as determined by calibration data						
	E1	D1	D2	D3	D4	D5
1>>	6.09 (D1)	2.554				
2>>	7.57 (D1)	4.877				
3>>	9.44 (D2)		.786			
	9.93 (D1)	5.092				
4>>	10.13 (D2)		3.048			
	11.19(D1)	3.956				
	11.52 (D2)		5.858			
5>>	14.52 (D1)	2.795				
	14.91 (D3)			.959		
6>>	15.62 (D2)		7.539			
	15.76 (D3)			4.256		
7>>	17.92 (D2)		5.545			
	18.13 (D3)			9.147		

Table 13b. Empirical Channel Boundaries - HEH-Princeton Data

Channel borders as determined by calibration data					
E1	D1	D2	D3	D4	D5
8>>					
<24.68 (D2)					
<24.68 (D4)					
9>>					
27.01 (D3)					
27.51 (D5)					
10>>					
34.61 (D3)					
35.01 (D5)					
11>>					
37.98 (D5)					
37.56 (D4)					
12>>					

Table 13c. Empirical Channel Boundaries - HEH-Harvard Data

Channel borders as determined by calibration data					
E1	D1	D2	D3	D4	D5
11>>					
37.9 (D4)					
41.0 (D5)					
12>>					
48.0 (D5)					
50.1 (D4)					
13>>					
52.9 (D4)					
54.6 (D5)					
14>>					
62.2 (D4)					
66.6 (D5)					
15>>					
73.1 (D4)					
73.1 (D5)					
16>>					
100.1 (D4)					
100.1 (D5)					

Table 14. Empirical Channel Boundaries - LEH

Channel borders as determined by calibration data					
	E1	LD1	LD2	LD3	LD4
1>>	1.029 (1)	.522			
	2.045 (2)		.670		
2>>	2.175 (1)	0.976			
	2.270 (2)		1.066		
3>>	2.58 (1)	.792			
	2.813 (3)			.666	
4>>	2.84 (1)	.716			
	3.160 (3)			1.376	
	3.23 (2)		.885		
5>>	4.035 (2)		.653		
	3.994 (4)				.668
6>>	4.71 (4)				2.225
	4.76 (3)			1.304	
7>>	7.639 (3)			.726	
8>>	9.24 (4)				3.036
	9.49 (1)	.249			
	9.99 (3)			.554	



Table 15. Empirical Channel Boundaries - Ions

Channel	EO	He	C	N	O	Fe
5>>	12.8	-	22.8	25.8	29.1	72.0
6>>	20.3	-	29.0	32.1	35.2	82.9
7>>	26.8	-	38.9	37.5	40.7	91.3
8>>	41.0	-	-	-	53.0	107.6
9>>	xxx					
10>>	xxx					
	xxx					

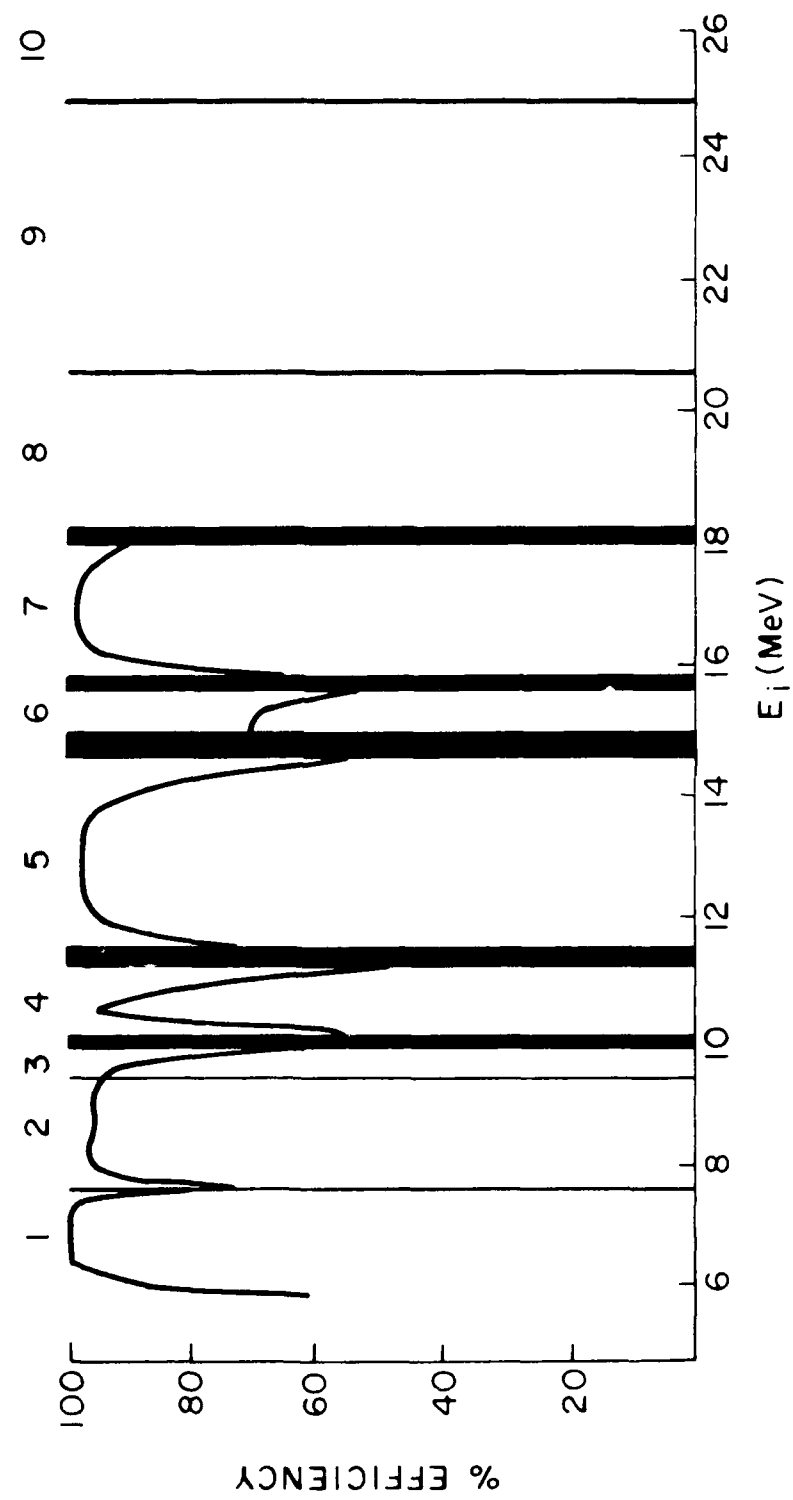


Figure 19. HEH Efficiency Curves

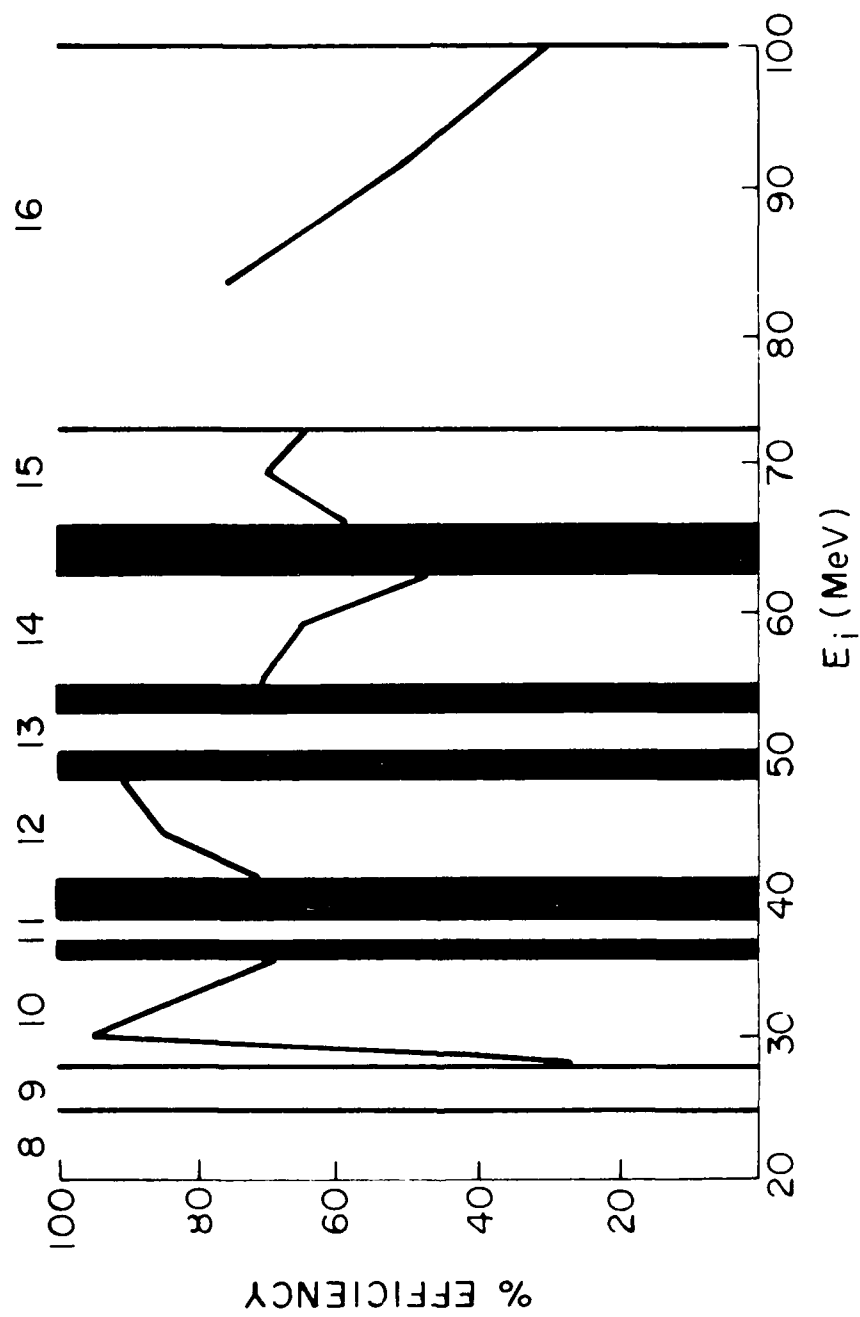


Figure 19. HEH Efficiency Curves (Cont.)

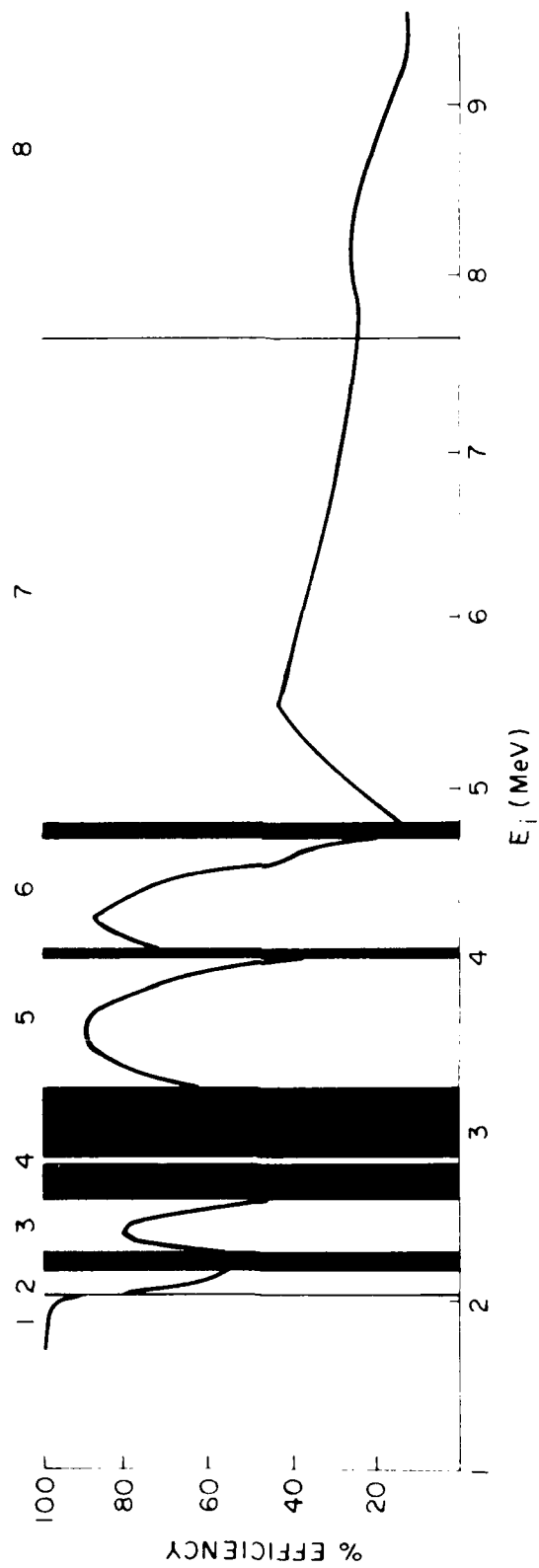


Figure 20. LEH Efficiency Curve

Table 16a. LEH Deposition Ratios

Ratio of designed to actual energy depositions in the detector at each boundary.									
ch.	<u>Pittsburgh Data</u>								
	0/1	1/2	2/3	3/4	4/5	5/6	6/7	7/8	Avg.
D1	1.075	1.021	xxx	1.057	1.050	1.031	xxx	xxx	1.047
D2	xxx	xxx	0.791	0.992	0.997	xxxx	1.026	1.015	0.964
D3	xxx	xxxx	xxxx	xxxx		0.937	1.007	1.01	0.985
ch.	<u>Princeton Data</u>								
	8/9	9/10	10/11	11/12	Avg.				
D2	1.004	xxx	xxx	xxx	1.004				
D3	xxx	1.026	1.009	xxx	1.02				
D4	0.772	1.064	xxx	1.012	0.95				
D5	xxxx	xxxx	1.555	1.017	1.286				
ch.	<u>Harvard Data</u>								
	11/12	12/13	13/14	14/15	15/16	Avg.			
D3	xxxx	xxxx	xxxx	xxxx	xxxx	xxxx			
D4	1.00	1.04	.98	1.00	1.00	1.00			
D5	.65	1.02	1.11	1.09	.99	.97			

Table 16b. HEH Deposition Ratios - Pittsburgh Data

Ratio of designed to actual energy depositions in the detector at each boundary.				
Boundary	D1	D2	D3	D4
0/1	1.09	xxx	xxx	xxx
1/2	xxx	1.37	xxx	xxx
2/3	1.03	1.06	xxx	xxx
3/4	1.07	xxx	1.34	xxx
4/5	1.10	0.93	1.07	xxx
5/6	xxx	0.97	xxx	1.37
6/7	xxx	xxx	0.97	1.02
7/8	xxx	xxx	1.19	xxx
8/-	0.95	xxx	0.91	0.96
Average:	1.05	1.08	1.10	1.12

Table 17. Average Channel Efficiencies

Average calibrated channel efficiencies (between the empirical channel boundaries) of each channel; from calibration data. Also listed are conversion rates from counts to flux; conversion factor is equal to (efficiency $\times$ geometric factor $\times$ actual channel width) <sup>-1</sup>					
<u>High Energy Head:</u>			<u>Low Energy Head:</u>		
Channel	Eff.	Conversion Factor	Channel	Eff.	Conversion Factor
1	90%	6.256	1	93%	87.47
2	87%	5.122	2	63%	1009.
3	78%	21.80	3	70%	380.9
4	74%	10.62	4	34%	9003.
5	86%	3.230	5	65%	166.4
6	60%	19.56	6	77%	159.0
7	86%	4.486	7	30%	95.69
8	76%	1.674	8	15%	344.1
9	80%	4.471			
10	70%	1.667			
11	55%	5.942			
12	82%	1.452			
13	79%	3.767			
14	63%	1.740			
15	61%	2.102			
16	55%	1.782			

Measurements also were made at the Harvard calibration facility with the head assemblies at a ten degree angle to the beam. The angle did not noticeably change the energy response, but the efficiency was lowered by almost a factor of ten. Background measurements were also made to check the response of the heads to proton beams incident from the side, and to high energy, low flux electrons incident from the front and from the side. In all these cases, the response of the instrument to these particles was negligible.

## **4. COMPUTER SIMULATIONS**

### **4.1 Introduction**

To facilitate the design of the discriminator logic, two different computer simulations of PROTEL were developed and used before and during the development of the instrument. The first, done by Emmanuel College Physics Research Division,<sup>19</sup> studied the probability of high count rate pulse pileup, during both normal and storm environments, for the low energy, high flux end of the proton environment. The other, done separately by both D. Brautigam and T. Jordan, studied the effects of range-energy straggling and other variations upon a simple continuous-slowing-down-approximation (CSDA) method of determining the proton energy losses in the detector thicknesses.

The results were used to refine the logic design and point out problems with the original design. The refinements included allowance for straggling depositions at the high end of the HEH range and the insertion of a low energy absorber in front of the LEH detector stack, to cut out high fluxes of low energy particles.

### **4.2 Pulse Pileup Simulation**

The pileup simulation was run only for the low energy end of the LEH incident energy range, the region of highest flux. The program used two sample environments, a typical spectrum for  $E > 0.79$  MeV at a McIlwain L shell of 3.0, and a typical storm spectrum for  $E > 0.79$  MeV. The result of the simulation was the determination that a low energy particle absorber was needed in front of the LEH detector stack to cut down the high fluxes of low energy protons that would otherwise swamp the electronics. To this end, a 0.35 mil thickness of aluminum was added to the LEH flight unit, and the detector logic changed accordingly. This absorber removes all incident protons of energy less than 750 keV.

### **4.3 Response Function Simulations**

Two programs were developed to model the response of the PROTEL instrument to various input spectra. They were used to determine, for the flight unit, the most efficient selection of detector

---

19. Brautigam, Don (1985, April) PROTEL Simulation Report, Emmanuel College Physics Research Division.



thicknesses and channel widths. One was developed by a consultant, Thomas Jordan, and used a Monte Carlo technique for calculating particle trajectories through the instrument. The other, developed by Emmanuel College Physics Research Division, was called STRAGGL, and used the range tables of J. Janni<sup>15</sup> and the energy straggling tables of Vavilov.<sup>20,21</sup> Both programs gave essentially the same result, so the simpler STRAGGL routine was used.

The STRAGGL routine asks for the configuration of the instrument in terms of detector thicknesses and channel boundaries. Then, given a particular input spectrum, it computes the response of the instrument to the spectrum by sending each incident particle through the stack of detectors, using the range tables to calculate energy losses in each detector, and adding random amounts of detector noise and straggling effects.

When the instrument was redesigned, just before the flight unit was constructed, the STRAGGL routine was used to optimize the choices of detector thicknesses and channel boundaries. Figures 21 and 22 show the modelled response to the final design. A comparison of these figures to the measured response curves shown in Figures 19 and 20 shows that the STRAGGL routine is a very good model. As a result, it will be very useful in deconvolving actual satellite data.

- 
20. Seltzer, S.M. and Berger, M.J. (1964) Energy Loss Straggling of Protons and Mesons: Tabulation of the Vavilov Distribution, *Studies in Penetration of Charged Particles in Matter*, Nuclear Science Series Number 39.
  21. Northcliffe, L.C. and Schilling, R.F. (1970) Range and Stopping-Power Tables for Heavy Ions, *Nuclear Data Tables A7*.

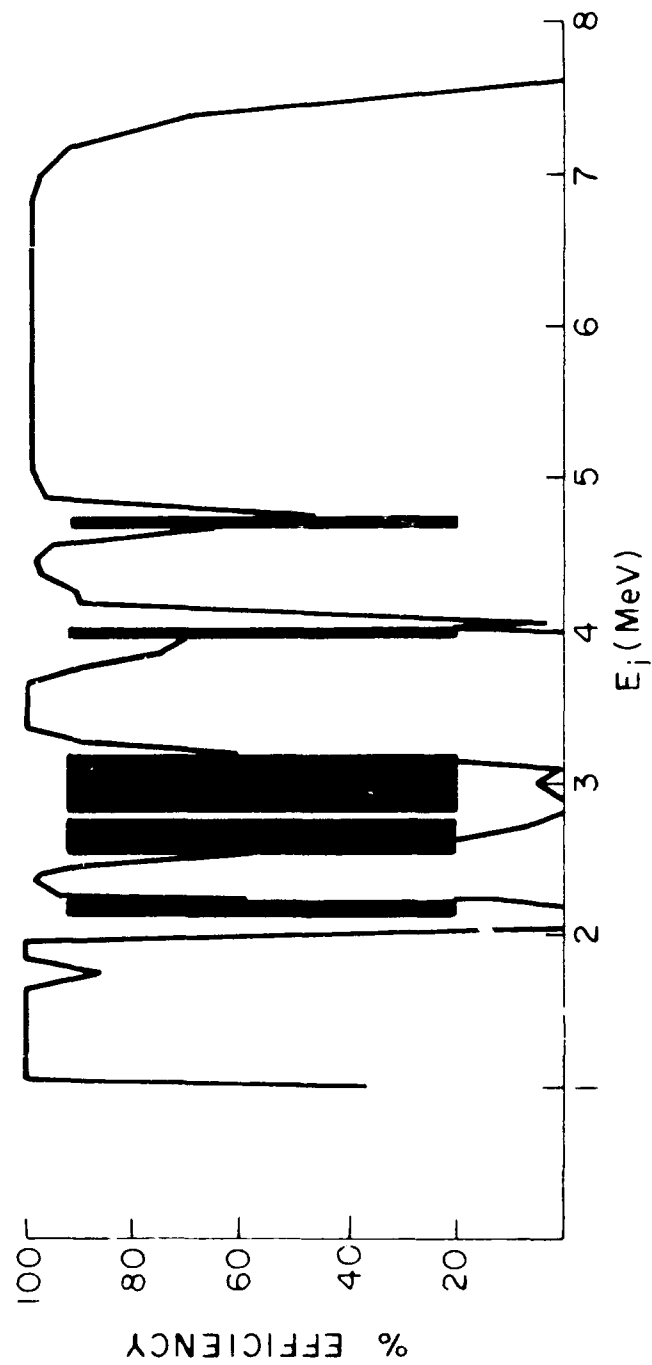


Figure 21. STRAGGL Routine Response for HEH

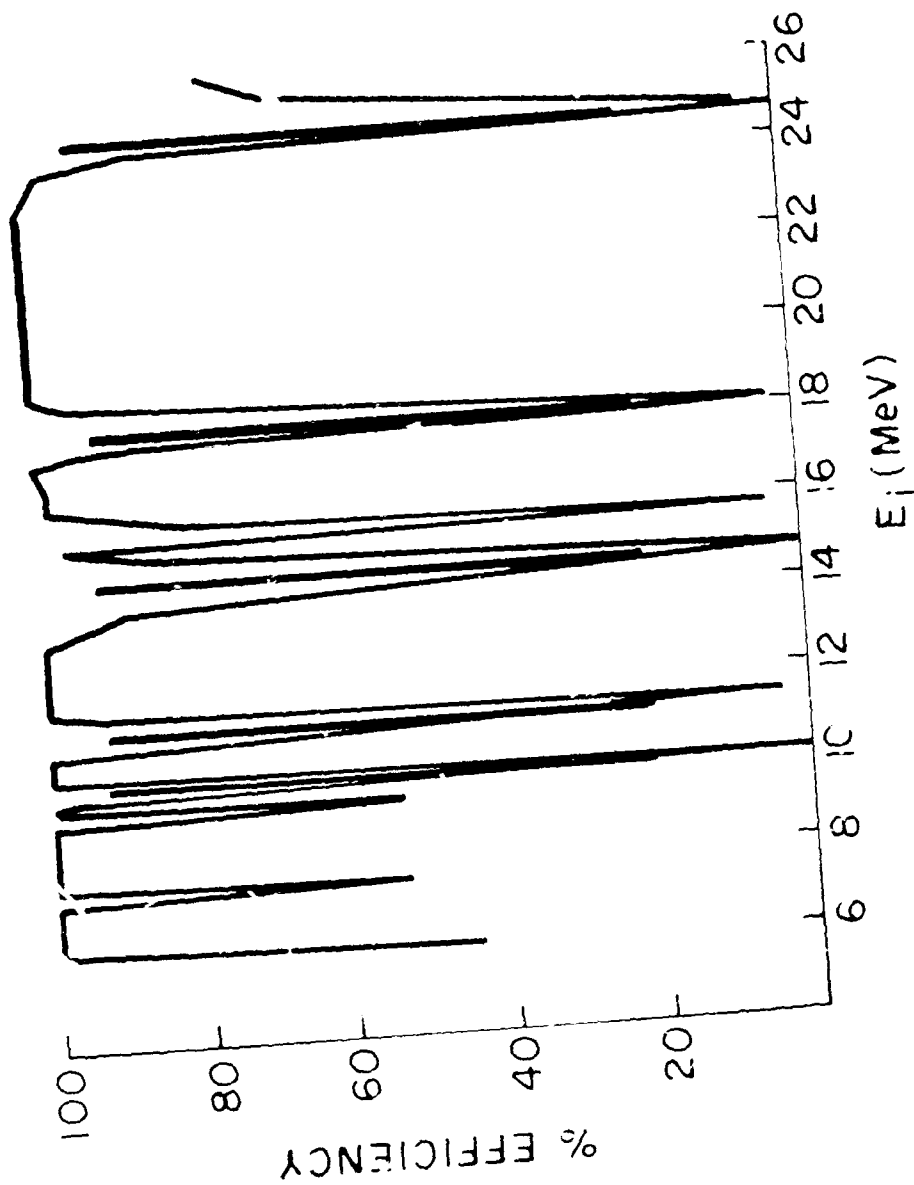


Figure 22. STRAGGL Routine Response for LEH

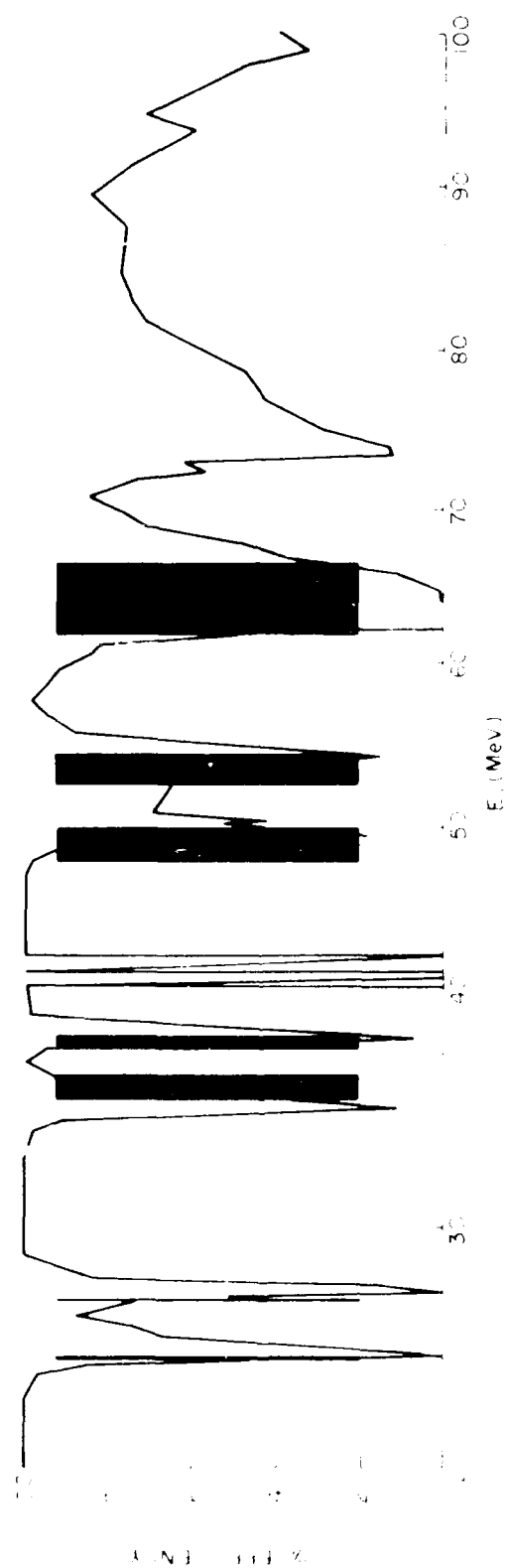


Figure 22. STRAGGL Routine Response for LEH (Cont.)

## References

1. Vette, J.L., Teague, M.J., Sawyer, D.M., and Chan, K.W. (1979) Modeling of the Earth's radiation belts, *Solar Terrestrial Predictions Proceedings* (Vol. 2), R.F. Donnelly, Ed., U.S. Dept. of Commerce, Washington, D.C.
2. Fischer, H.M., Auschrat, V.W., and Wibberenz, G. (1977) Angular distribution and energy spectra of protons of energy  $5 < E < 50$  MeV at the lower edge of the radiation belt in equatorial latitudes, *J. Geophys. Res.* **82**:537.
3. Reagan, J.B., Bakke, J.C. Kilner, J.R. Mathews, J.D., and Imhoff, W.L. (1972) A high-resolution multiple-particle spectrometer for the measurements of solar particle events, *IEEE Trans. Nucl. Sci.* **NS-19**:554.
4. Morel, P.R., Hanser, F.A., and Sellers, B. (1974) *A Satellite Telescope for Protons and Alphas*, Panametrics, Inc., Waltham, Mass., Final Report for AFCRL-TR-74-0531, AD A003727.
5. Parsignault, D.R., Holeman, E., and Filz, R.C. (1981a) Solar cycle induced modulation of the 55 MeV proton fluxes at low altitudes, *J. Geophys. Res.* **86**:11493.
6. Parsignault, D.R., Holeman, E., and Filz, R.C. (1981b) Long term intensity decrease in the 8- to 25- MeV proton fluxes at low L values, *J. Geophys. Res.* **86**:11447.
7. Belian, R.D., Baker, D.N., Higbie, P.R., and Hones, E.W., Jr. (1978) High-resolution energetic particle measurements at  $6.6 R_E$ . 2. High-energy proton drift echoes, *J. Geophys. Res.* **83**:4857.
8. Baker, D.N., Belian, R.D., Higbie, P.R., and Hones, E.W., Jr. (1979) High-energy magnetospheric protons and their dependence on geomagnetic and interplanetary conditions, *J. Geophys. Res.* **84**:7138.
9. Brown, W.L., Higgenbotham, W.A., Miller, G.L., and Chase, R.L. (1969) *Semiconductor Nuclear-Particle Detectors and Circuits*, National Academy of Sciences, Publication 1594, Washington, D.C.
10. Knoll, G. (1979) *Radiation Detection and Measurement*, John Wiley and Sons, New York, N.Y.
11. EG&G Ortec, *Silicon Charged Particle Radiation Detectors Instruction Manual*, EG&G Ortec, Oak Ridge, Tennessee.
12. Sullivan, J.D. (1971) Geometrical factors and directional response of single and multi-element particle telescopes, *Nuclear Instruments and Methods* **95**:5.

13. Knoll, G. (1979) *Radiation Detection and Measurement*, John Wiley and Sons, New York, N.Y., p. 386.
14. Knoll, G. (1979) *Radiation Detection and Measurement*, John Wiley and Sons, New York, N.Y., p. 415.
15. Janni, J.F. (1982) Proton range-energy tables, 1 keV - 10 GeV, *Atomic Data And Nuclear Data Tables* **27**:4/6.
16. CRRES ICD (7 March 1989) Revision G, Ball Space Systems Division, Boulder CO.
17. Compliance Data Package for PROTEL, Ball Space Systems Division, Boulder, CO.
18. Military Standard 461B.
19. Brautigam, Don (1985, April) PROTEL Simulation Report of Emmanuel College Physics Research Division.
20. Seitzer, S.M. and Berger, M.J. (1964) Energy Loss Straggling of Protons and Mesons: Tabulation of the Vavilov Distribution, *Studies in Penetration of Charged Particles in Matter*, Nuclear Science Series Number 39.
21. Northcliffe, L.C. and Schilling, R.F. (1970) Range and Stopping-Power Tables for Heavy Ions, *Nuclear Data Tables A7*.